AD 285 630

AFCRL-62-672

NEW YORK UNIVERSITY

College of Engineering

RESEARCH DIVISION

University Heights, New York 53, N. Y.

Department of Meteorology and Oceanography

MESOSPHERE DYNAMICS

Final Report

Contract No. AF 19(604)-5492

Prepared by

Julius London
Katsuyuki Ooyama
Cuddapah Prabhakara

The research reported in this document has been sponsored by
GEOPHYSICS RESEARCH DIRECTORATE
AIR FORCE CAMBRIDGE RESEARCH LABORATORIES
OFFICE OF AEROSPACE RESEARCH
UNITED STATES AIR FORCE
BEDFORD, MASSACHUSETTS

May 1962

AFCRL-62-672

RESEARCH DIVISION
COLLEGE OF ENGINEERING
NEW YORK UNIVERSITY

MESOSPHERE DYNAMICS

Final Report

Contract No. AF 19(604)-5492

Prepared by

Julius London
Katsuyuki Ooyama
Cuddapah Prabhakara

Project No. 8604
Task No. 86044

The research reported in this document has been sponsored by
GEOPHYSICS RESEARCH DIRECTORATE
AIR FORCE CAMBRIDGE RESEARCH LABORATORIES
OFFICE OF AEROSPACE RESEARCH
UNITED STATES AIR FORCE
BEDFORD, MASSACHUSETTS

Department of Meteorology and Oceanography

May 1962

Table of Contents

Table of Contents (Cont.)

List of Figures

List of Figures (Cont.)

Preface

The following report covers a discussion of the research done on the Mesosphere Dynamics Project, Contract No. AF 19(604)-5492, during the life of the project, 1 May 1959 to 30 November 1961.

The efforts of the project were directed towards study of the dynamics and thermodynamics of the stratosphere and mesosphere. Because of the fundamental role played by ozone to problems in this region of the atmosphere, research related to the formation, observation, and distribution of ozone became of central interest to the project. The research is reported in three parts:

Part I: Accuracy of the determination of the vertical distribution of atmospheric ozone by the infrared method, by Katsuyuki Ooyama.

The vertical distribution of atmospheric ozone as determined by the infrared method is limited in vertical resolution and is very sensitive to observational errors. A set of linearized error equations was derived from the three basic equations of the infrared method, and the sensitivity of the determined ozone distribution to errors in the observational input data (total ozone, infrared absorption, and infrared emission) was computed for a few cases. It was shown that in the region above the tropopause, the ozone distribution is most sensitive to measurements of infrared absorption. An estimate was made of the accuracy of the inverted use of the Curtis-Godson approximation in obtaining the mean pressure of the ozone distribution.

Part II: Absorption processes in the stratosphere and mesosphere, by Julius London and Cuddapah Prabhakara.

The photochemical equilibrium distribution of ozone was computed for various latitudes for summer and winter and the absorption of solar radiation by ozone and molecular oxygen was calculated. It was found that the absorption by ozone in the atmosphere below 80 km was everywhere larger than that by molecular oxygen. The region of maximum absorption per unit mass was shown to coincide with the stratopause.

Part III: The distribution of total ozone over the Northern Hemisphere, by Julius London.

Maps of the distribution of total ozone over the Northern Hemisphere were analyzed for the whole year and for each of the four seasons from data accumulated over the period 1926-1959. The analysis showed marked longitudinal variations of total ozone even for the annual average. Ozone ridges appear well developed over Eastern North America, Eastern Asia, and Central Europe. The hemispheric distribution of total ozone was shown to be related to the atmospheric circulation in the upper troposphere and lower stratosphere.

In addition to those mentioned above, Mr. James Neiger and Capt. Robert Simonson contributed substantially in time and effort to the accomplishments of the project.

PART I

Accuracy of the Determination of the Vertical Distribution of Atmospheric Ozone by the Infrared Method

by

Katsuyuki Ooyama

ABSTRACT

The vertical distribution of atmospheric ozone as determined by the infrared method is limited in vertical resolution and is very sensitive to observational errors. A set of linearized error equations was derived from the three basic equations of the infrared method, and the sensitivity of the determined ozone distribution to errors in the observational input data (total ozone, infrared absorption and infrared emission) was computed for a few cases. It was shown that in the region above the tropopause, the ozone distribution is most sensitive to measurements of infrared absorption. The numerical results indicate that a positive error of, e.g., one percent in the observation of infrared absorption could erroneously increase the ozone amount in the layer tropopause to 50 mb by 15 percent and erroneously decrease the amount of ozone in the layer 50-30 mb by about 10 percent.

In the infrared method the Curtis-Godson approximation is used in an inverted way in order to obtain the mean pressure of the ozone distribution. An estimate of the accuracy of the inverted use of the approximation was made by making use of a simple spectral model, and the effect of this theoretical error on the determined ozone distribution was also included in the above error analysis. The mean pressure was found to be underestimated by about 20 percent in the case of atmospheric ozone, and the resulting ozone distribution would be severely distorted by this error alone.

1. Introduction

Although the total amount of atmospheric ozone in a vertical column is now observed daily at many stations over the world, the usefulness of ozone observations in the study of atmospheric motion, especially in the stratosphere, would be radically increased if the vertical distribution of ozone were observed on a synoptic basis. Among the several methods of observation which have been developed, direct methods by sending apparatus aloft are preferable in terms of potentially obtainable accuracy. Nevertheless, until the time when more and inexpensive ozonesondes become available, indirect methods such as the Umkehr and the infrared methods may continue to be important means of supplying needed data of the vertical ozone distribution.

The infrared method as discussed in this paper is basically the same as that recommended by the International Ozone Commission (1956) and as described by Goody and Roach (1956). A variation of this method, particularly of the computational procedure, was proposed by Vigroux (1959). Empirical comparison of the vertical ozone distributions determined by Vigroux with those which were simultaneously determined by other methods -- chemical and optical ozonesondes, and Umkehr -- were recently published by Brewer, Dütsch, Milford, Migeotte, Paetzold, Piscalar, and Vigroux (1960). A visual inspection of the results reveals that the values of the ozone density at any level which are determined by the different methods often differ by 50 percent or more. Goody and Roach (1956) showed that the ozone distribution in the stratosphere as determined by the infrared method was extremely sensitive to the error in the absorption measurement in the

9.6μ ozone band. As a result, the British group aimed at determination of only the tropospheric ozone amount from the measurement of emission intensity in the 9.6μ band (Goody and Roach, 1958; Walshaw, 1960).

Another method of determining the vertical ozone distribution from infrared observations was independently developed, and a long series of observations at Flagstaff, Arizona was analyzed by Epstein, Osterberg, and Adel (1956). This method was based on the same principles as that of Goody and Roach, but it is now considered obsolete (Epstein, 1957) partly because of an improper assumption on the pressure dependency of the infrared absorption by atmospheric ozone. The study reported here originated in our effort to reanalyze the unique set of Flagstaff observational data by the method recommended by the International Ozone Commission. Unfortunately, the attempt at reanalysis had to be abandoned because of the strong suspicion that systematic errors were present in the observational data for which no reliable correction procedure could be found.

The purpose of this paper is to make a theoretical analysis of the accuracy of the determination of the vertical distribution of atmospheric ozone by the infrared method. The error analysis of the determined ozone distribution is made in terms of the errors in observational data and also in the inverted Curtis-Godson approximation. Although technical aspects of the infrared observations are not discussed here, the result of the error analysis will be a guide to those who may plan to make such observations. Since the ozone distribution, particularly in the stratosphere, is found to be very sensitive to observational errors, this fact should be borne in mind by those who are mainly interested in results obtained by the infrared method.

2. Formulation of the infrared method

Absorption due to the 9.6μ band of ozone, like infrared absorption due to other gases, depends on the total pressure as well as the amount of ozone present. When the absorption due to ozone takes place at a uniform pressure, the absorption is simply a function of the amount of ozone m, and the uniform pressure p, along the path (the temperature effect is small and will be neglected here). Laboratory measurements of the 9.6μ ozone band absorption along uniform pressure paths were made by Summerfield (1941) and by Walshaw (1957). Walshaw expressed the absorption in terms of integrated absorptivity over the entire band which is called by him the band area, and the effective band width by some others; the unit being wave number per cm. Walshaw's laboratory measurements will be used as the basis of the following analysis, and his empirical result is specifically written

$$\bar{A} = W(m, p) \qquad (1)$$

where $\bar{A}$ is the integrated absorptivity along a uniform pressure path, and $W(m, p)$ is the empirically determined function shown in Fig. 1.

In the case of absorption of solar radiation in the same band by atmospheric ozone, the absorption takes place in a path along which atmospheric pressure is not uniform, and the resulting absorption depends on the ozone distribution with respect to pressure.

There are several ways of representing the vertical distribution of ozone. The commonly used ozone density (ozone mass per unit geometrical volume) is inconvenient for theoretical manipulation. The ozone mixing ratio, which varies by many orders of magnitude through the ozone layer, is not particularly suitable for a graphical representation

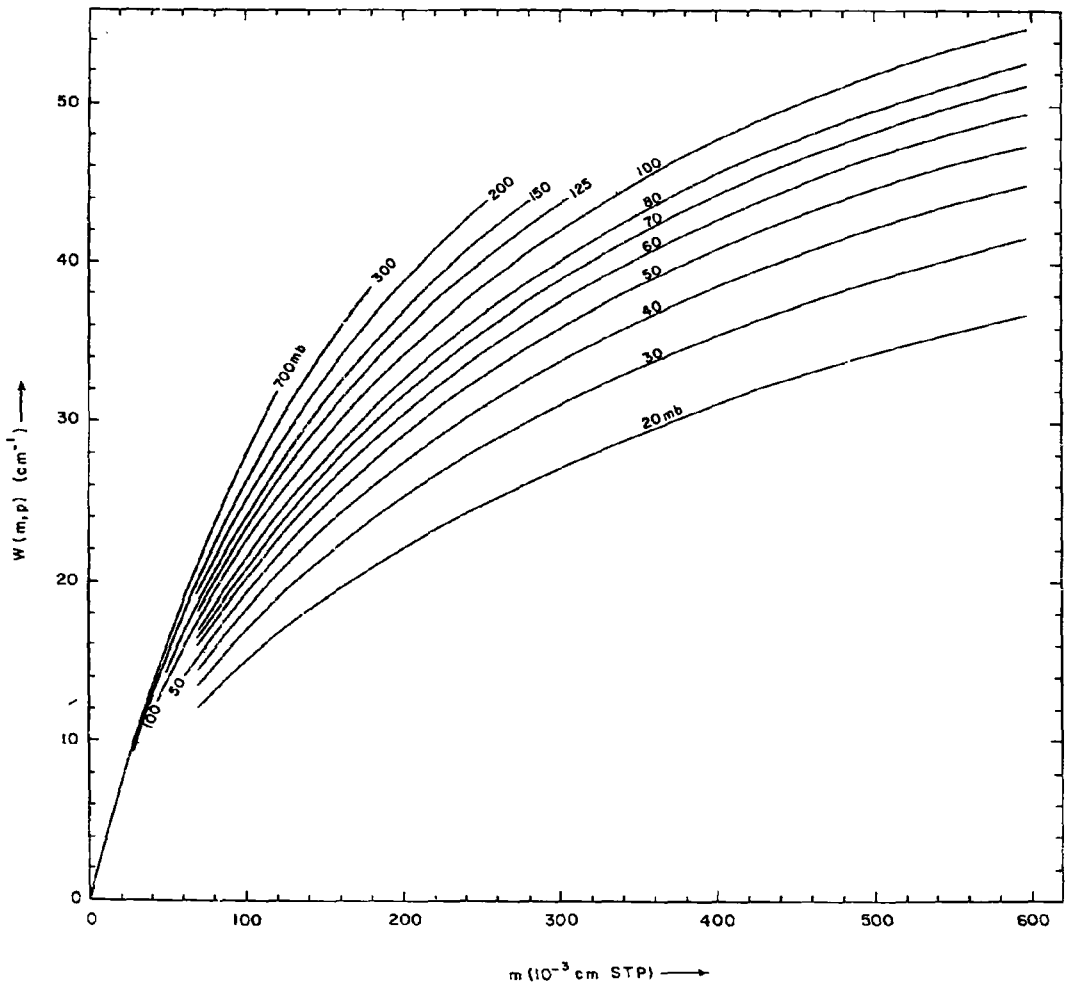

Figure 1. The integrated absorptivity (band area), W(m, p), of the 9.6μ band of ozone in uniform-pressure paths. Curves are drawn according to the empirically determined interpolation formulas of Walshaw (1957).

or numerical calculation. We shall use, as the primary quantity describing the vertical ozone distribution, a pseudo ozone density defined on a logarithmic pressure scale. The exact definition is given in the following.

In order to retain the advantage of using atmospheric pressure as the vertical coordinate, we introduce a pressure-height h, defined by

$$h = -\bar{H}\,\ell n(p/p_o)\,, \tag{2}$$

where p is the atmospheric pressure, p_o is the pressure at the ground, and $\bar{H}$ is a constant having the dimension of length. Although the constant $\bar{H}$ can be chosen completely arbitrarily, it is assumed here that $\bar{H}$ is the scale height corresponding to a temperature of 220°K. Then h is only approximately equal to geometric height. However, since the difference between the pressure-height and geometric height is not of much importance here, we may simply call h "height". The pressure p, now is considered to be a function of the new independent variable h, i. e.,

$$p(h) = p_o \exp(-h/\bar{H})\,. \tag{3}$$

We define the cumulative ozone distribution function m(h), as the amount of ozone in a vertical column of unit cross section between the ground and an arbitrary level at h, and also define the pseudo ozone density u(h), by

$$u(h) = dm/dh\,. \tag{4}$$

If m(h) is measured in cm STP and h in km, the unit of u(h) is cm STP per km. Because of the above choice of $\bar{H}$, the pseudo density, u(h), is nearly equal to the true ozone density in the lower stratosphere. The true density at any height is given by $(\bar{H}/H)\,u(h)$, where H is the

scale height corresponding to the temperature at the height under consideration. The ozone mixing ratio can easily be shown to be proportional to $u(h)/p(h)$.

When any particular ozone distribution is given, the integrated absorptivity of the 9.6μ band due to that part of the ozone along a path between the ground and any level h, which is denoted by A(h), is an increasing function of h. However, A(h) is a function of the ozone distribution itself, in the sense that A(h) depends on all values of $u(h')$ in the interval $0 \leq h' \leq h$. No laboratory measurements of the absorption along such a variable pressure path have been made, and theoretical calculations of A(h) based on the detailed spectrum of the 9.6μ band are not practical. However, it was shown by Curtis (1952) that in the case of water vapor in the atmosphere, the absorption along a variable pressure path could be approximated by the absorption along a uniform pressure path of the same amount of absorber at the mean pressure of the mass distribution of the absorber. A similar method of approximation, including also the temperature effect, was independently developed by Godson (1955). Although Curtis indicated that the approximation is less accurate in the case of atmospheric ozone whose typical vertical distribution is quite different from that of water vapor, the use of the Curtis-Godson approximation was recommended by the International Ozone Commission (1956) on the ground that no better approximation was available. Under this approximation, we have for a vertical path

$$A(h) \simeq W[u(h), q(h)] \tag{5}$$

Here, the two arguments of Walshaw's empirically determined function

W(m, p) have been replaced, respectively, by the two functions of h: the amount of ozone in the layer below the level h which is given by

$$m(h) = \int_0^h u\,dh \,, \tag{6}$$

and the mean pressure of the ozone distribution in the same layer which is defined by

$$q(h) = \left[\int_0^h pu\,dh\right] \Big/ m(h) \tag{7}$$

If an exact equality is to be assumed, (5) should be considered as the definition of the spectroscopic mean pressure, $q_s(h)$, namely

$$A(h) = W[m(h), q_s(h)] \tag{8}$$

The Curtis-Godson approximation, as introduced by the authors, meant that

$$W[m(h), q_s(h)] \cong [m(h), q(h)] \tag{9}$$

However, in the infrared method as recommended by the International Ozone Commission, a tacit assumption is made that

$$q_s(h) \cong q(h) \tag{10}$$

is a good approximation in addition to (9). The approximation of this form will be called the inverted Curtis-Godson approximation, and its accuracy will be discussed in Section 4. Meanwhile, it may be stated here that that validity of approximation (10) does not necessarily follow from that of (9) and that the former is much poorer than the latter particularly when the whole ozone layer ($h = \infty$) is concerned.

Atmospheric ozone at every height emits radiation in the 9.6μ band according to its own temperature. The emission intensity in the

9.6μ band, E(h), which is due to ozone in the layer below the level h, and which reaches the ground vertically, may be given by

$$E(h) = \int_0^h B(h) \frac{dA(h)}{dh} dh \qquad (11)$$

where B(h) is the average black body emission intensity over the 9.6μ band at the temperature at each height h. The vertical distribution of temperature is considered to be known either from radiosonde observation or by assumption, so that the black body intensity in each case is a known function of h.

In the case of oblique incidence, as observations are generally made, u(h) and m(h) in the above formulas have only to be multiplied by the secant of the zenith angle of the path. For the sake of simplicity, but without loss of general validity of the results, it is assumed that observations are made with vertical incidence. The three observational data from which a vertical ozone distribution is to be determined are the total amount of ozone $m(\infty)$, the integrated absorptivity of the 9.6μ ozone band $A(\infty)$, and the emission intensity $E(\infty)$ due to ozone in the entire column from the ground to the top of the atmosphere. The spectroscopic mean pressure of the entire column, $q_s(\infty)$, is immediately determined from the observed values of $m(\infty)$ and $A(\infty)$ by definition (8).

The problem is formulated so as to determine the function u(h), from the three integrals:

The total ozone

$$\int_0^\infty u(h)dh = m(\infty) \qquad (12)$$

the mean pressure under approximation (10)

$$\int_0^\infty p(h)\, u(h)\, dh \simeq m(\infty)\, q_s(\infty) \tag{13}$$

and the emission intensity

$$\int_0^\infty B(h)\, \frac{dA(h)}{dh}\, dh = E(\infty) \tag{14}$$

where A(h) is related to u(h) by (5), (6), and (7). It is evidently impossible to determine a unique solution u(h) from a finite number of integrals. What we may attempt is to restrict ourselves to seek a solution within a preselected class of functions which contain only three independent parameters, and to solve for the parameters.

According to the recommendation of the International Ozone Commission, the atmosphere is divided into four layers. The ozone distribution in the top layer above the 10 mb level is assumed known. The ozone mixing ratio (consequently, u(h)) in each of the three lower layers is assumed to be proportional to a given function of pressure. The parameters of the ozone distribution in this model are the amounts of ozone in the three lower layers. The assumed linear dependency of u(h) on those parameters facilitates calculation of a solution. The resulting ozone density profile, however, generally shows discontinuities at the boundaries of the layers, so that some degree of subjectivity is left when the ozone density curves are to be smoothed. Vigroux (1959) modified the above scheme to obtain a continuous distribution objectively. The number of parameters in Vigroux's model is six, although only three of these are independent, and the numerical procedure used in solving the equations is rather complex. There may be other models, but it is not our purpose to discuss which model is best. Choice of a model, i.e., selection of the type of functions as possible solutions must be made

inevitably by a subjective judgment (or, by an objective judgment based on subjectively chosen rules) on how well the model fits the whole variety of real distributions of atmospheric ozone. Whichever model is chosen, however, it is not possible to reproduce most details of the vertical ozone distribution. Only a broad profile may be obtained by adjusting the three independent parameters in the model. One might expect that this limit of resolution would be improved by taking infrared observations at different zenith angles and thus by supplying more than three integrals involving the unknown function u(h). However, since the accuracy of the infrared observations must, as is shown in the following section, be about one order of magnitude better than the desired accuracy of the determined ozone distributions in the stratosphere, observations taken at different zenith angles can hardly be considered as independent information, unless a marked improvement is introduced in correcting the raw observational data for the influence by absorbers other than ozone.

Therefore, if the low limit of vertical resolution obtainable by the infrared method is accepted, any reasonable model may be selected. Then, when the observational data are supplied, the vertical ozone distribution can be "uniquely" determined.

A serious question still remains concerning the accuracy of an ozone distribution thus determined, if inevitable errors in the observational data are taken into account.

3. Error analysis

3.1 Mathematical development

Assume that u(h) represents the true vertical ozone distribution and that $m(\infty)$, $A(\infty)$, and $E(\infty)$ are the basic observational data which would be obtained for the ozone distribution u(h) if there were no observational errors. Suppose that, for some reason, we obtain from actual observations slightly different values $m(\infty) + \delta m(\infty)$, $A(\infty) + \delta A(\infty)$, and $E(\infty) + \delta E(\infty)$, which would be the correct data if the ozone distribution were $u(h) + \delta u(h)$. We will assume that the relative errors in the observed data are sufficiently small so that $|\delta u(h)/u(h)| << 1$ for all h.

The equation for total ozone is now written

$$\int_0^\infty (u + \delta u)dh = m(\infty) + \delta m(\infty)$$

or, because of (12),

$$\int_0^{h_{10}} \delta u\, dh = \delta m(\infty) - \int_{h_{10}}^\infty \delta u\, dh \qquad (15)$$

where h_{10} is the height of the 10 mb level. As described in the preceding section, the ozone distribution above the 10 mb level is, in the infrared method, assumed to be known. If the assumed distribution is not correct, the integral on the right-hand side generally does not vanish, and this error in the assumption, along with the observational error $\delta m(\infty)$, is compounded into an erroneous estimate of the ozone distribution in the layer below the 10 mb level. Although we recognize the different causes of these terms on the right-hand side, they are practically inseparable. Therefore, we may simply absorb the second

term into the first by writing

$$\int_0^{h_{10}} \delta u \, dh = \delta m(\infty) \tag{16}$$

From the definition given by (7), we have

$$\int_0^{\infty} pu \, dh = m(\infty)\, q(\infty)$$

However, $q(\infty)$ is not obtainable from observations. Instead, $q_s(\infty)$ is determined from the observations and substituted for $q(\infty)$ under the inverted Curtis-Godson approximation (10). Therefore, even if no observational error exists, a certain error is made in estimating $q(\infty)$. Instead of the approximate equality (10), we may specifically write

$$q_s(\infty) = q(\infty) + \delta_c\, q(\infty) \tag{17}$$

where $\delta_c\, q(\infty)$ is the error due to the use of approximation (10). Since $q_s(\infty)$ is obtained from $A(\infty)$ and $m(\infty)$ by the definition given in (8), any error in the latter quantities will give rise to an error in $q_s(\infty)$; i.e.,

$$A(\infty) + \delta A(\infty) = W[m(\infty) + \delta m(\infty), q_s(\infty) + \delta q_s(\infty)].$$

Expanding the right-hand side in a Taylor series and neglecting higher order terms of small quantities, we obtain

$$\delta q_s(\infty) = \left(\frac{\partial W}{\partial q}\right)_\infty^{-1} \left[\delta A(\infty) - \left(\frac{\partial W}{\partial m}\right)_\infty \delta m(\infty)\right] \tag{18}$$

where the subscript ∞ indicates that the partial derivatives are evaluated at $m = m(\infty)$ and $q = q(\infty)$. (Since we consider only the first order terms, the difference in the values of the derivatives at $q = q_s(\infty)$ and $q(\infty)$ is neglected.) Combining both types of error, we now have in lieu of (13)

$$\int_0^\infty p(u + \delta u)dh = [m(\infty) + \delta m(\infty)][q(\infty) + \delta_c q(\infty) + \delta q_s(\infty)]$$

or, again neglecting higher order terms and substituting (18), into the expression above we have

$$\int_0^{h_{10}} p\,\delta u\,dh = [q(\infty)\,R(\infty)/S(\infty)\,\delta m(\infty) + [1/S(\infty)]\,\delta A(\infty) + m(\infty)\,\delta_c q(\infty) \quad (19)$$

where $R(\infty)$ and $S(\infty)$ are the particular values at $h = \infty$ of more generally defined functions

$$R(h) \equiv R[m(h), q(h)] = \left(\frac{\partial W}{\partial m} - \frac{q}{m}\frac{\partial W}{\partial q}\right)_h$$

and (20)

$$S(h) \equiv S[m(h), q(h)] = \left(\frac{q}{m}\frac{\partial W}{\partial q}\right)_h$$

These derived functions are shown in Fig. 2 as functions of m and p. In order to obtain R or S as a function of h, it is necessary only to draw a curve of $m = m(h)$ and $p = q(h)$ with h as a parameter. In (19) we have neglected the term

$$\int_{h_{10}}^\infty p\,\delta u\,dh$$

which arises for the same reason as the last term in (15) but is found by conservative estimate to be minor compared to the right-hand terms of (19).

When the error $\delta E(\infty)$, in the observation of emission intensity is considered, the equation corresponding to (14) is written

$$\int_0^\infty B\,\frac{d(A + \delta A)}{dh}\,dh = E(\infty) + \delta E(\infty)$$

After integration by parts and rearrangement of the terms, it may be written

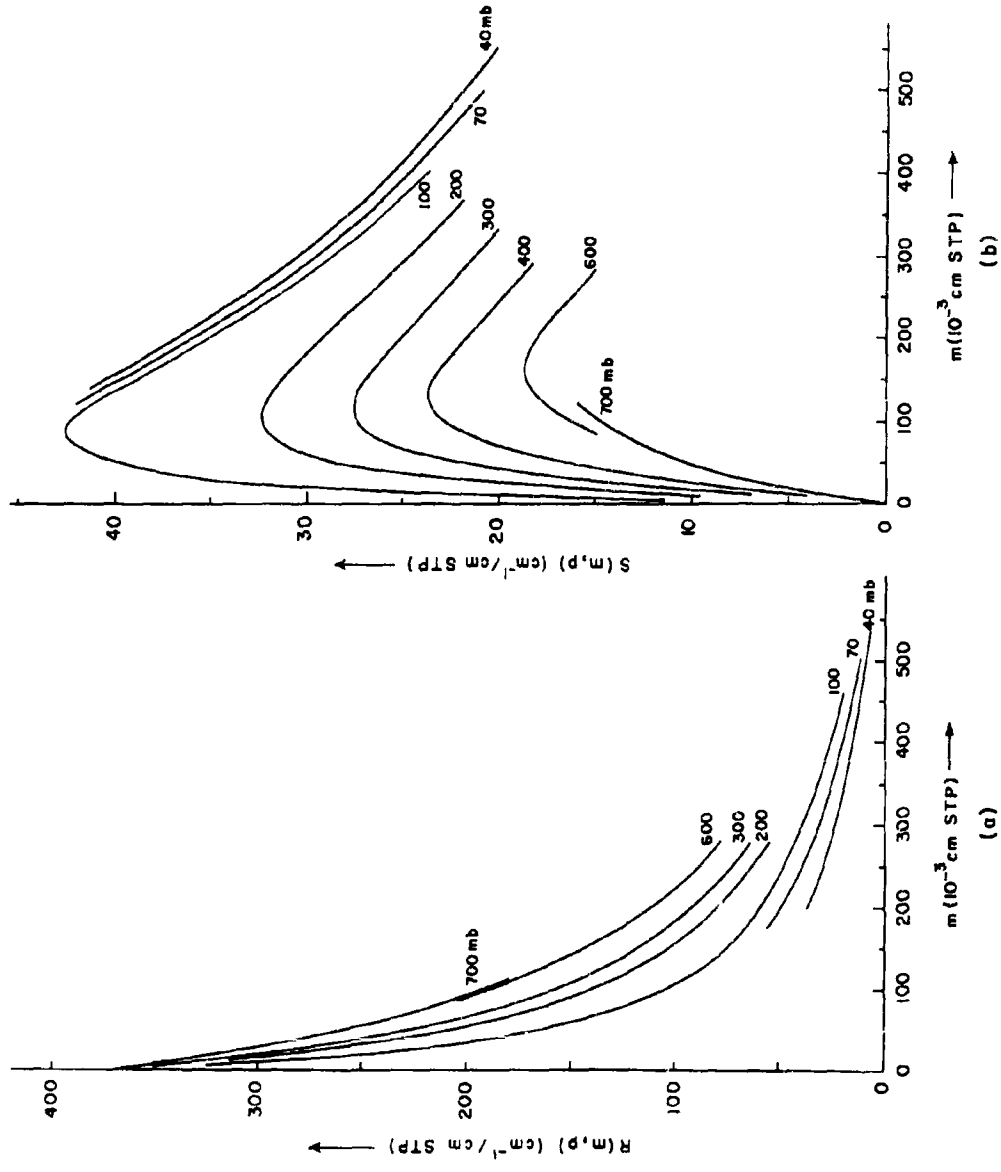

Figure 2. Derived functions of W(m, p) : (a) R(m, p). and (b) S(m, p). For definitions, see Eq (20) in the text.

$$-\int_0^{h_{10}} \frac{dB}{dh}\,\delta A\,dh = \delta E(\infty) - B(h_{10})\,\delta A(\infty) - \int_0^{h_{10}} [B(h) - B(h_{10})]\,\frac{d\delta A}{dh}\,dh \qquad (21)$$

The third term on the right-hand side depends on the possible error in the assumed ozone distribution above the 10 mb level, and also, to some degree, on the error in the computed ozone distribution below this level. An estimate of this term is difficult to obtain in actual cases, although because of the increasing temperature upward, it might amount to a few percent of $E(\infty)$. We shall again assume, as we did in connection with (15), that the third term is absorbed into the first term, $\delta E(\infty)$.

Since the Curtis-Godson approximation has better accuracy in estimating the absorption than in estimating the mean pressure, the approximation in the form of (9) may be used in order to express δA of the integrand on the left-hand side of (21) in terms of δu. By again neglecting higher order terms in the Taylor expansion, we have

$$\delta A(h) = \left(\frac{\partial W}{\partial m}\right)_h \delta m(h) + \left(\frac{\partial W}{\partial q}\right)_h \delta q(h) = R(h) \int_0^h \delta u\,dh + [S(h)/q(h)] \int_0^h p\,\delta u\,dh$$

Integration of (21) by parts after substitution of δA gives

$$\int_0^{h_{10}} G(h)\,\delta u\,dh = \delta E(\infty) - B(h_{10})\,\delta A(\infty) \qquad (22)$$

where the weighting factor

$$G(h) = -\int_0^{h_{10}} R(h)\,\frac{dB}{dh}\,dh - p(h) \int_0^{h_{10}} \frac{S(h)}{q(h)}\,\frac{dB}{dh}\,dh \qquad (23)$$

can be numerically computed once the ozone distribution, $u(h)$, and temperature distribution are specified.

(16), (19), and (22) relate three different weighted integrals of $\delta u(h)$ with the observational and theoretical errors on the right-hand sides. It is not possible to solve these equations for $\delta u(h)$ as an

arbitrary function of h, but as explained before, the values of three parameters, which specify a solution $\delta u(h)$ under a pre-selected model, can be determined.

The model which is chosen here for numerical examples (except case A') is similar to that recommended by the International Ozone Commission. The atmosphere below the 10 mb level is divided into three layers, designated by Δ_1, Δ_2, and Δ_3, and the unknown parameters are the errors of the amount of ozone in each layer:

$$\delta x_i = \int_{\Delta_i} \delta u \, dh \qquad (i = 1, 2, 3) \tag{24}$$

The "true" amount of ozone in each layer

$$x_i = \int_{\Delta_i} u \, dh \qquad (i = 1, 2, 3)$$

is a known quantity, since u(h) is considered here to be given.

As to variation of δu with respect to h, δu is assumed within each layer to be proportional to a certain power of pressure p; namely, in each Δ_i,

$$\delta u(h) = \delta x_i \, p^{a_i}(h) \Big/ \int_{\Delta_i} p^{a_i} \, dh \tag{25}$$

A description of the layers and the values adopted for a_i is given in Table 1 .

Table 1 . Details of the model

Layer, i	Interval Δ_i	a_i
1	ground (1000 mb) to tropopause	0
2	tropopause to 50 mb	-1
3	50 mb to 10 mb	0.8

Substitution of (25) into (16), (19), and (22) leads to linear algebraic equations for δx_i, which may be more conveniently written in a non-dimensional form by considering relative errors, $\delta x_i/x_i$, $\delta m(\infty)/m(\infty)$, etc. We put the relative error of the amount of ozone in each layer

$$y_i = \delta x_i/x_i \qquad (i = 1, 2, 3)\,, \tag{26}$$

the relative observational errors

$$z_1 = \delta m(\infty)/m(\infty), \quad z_2 = \delta A(\infty)/A(\infty), \text{ and } \quad z_3 = \delta E(\infty)/E(\infty), \tag{27a}$$

and the relative error of the mean pressure due to the use of the inverted Curtis-Godson approximation

$$z_4 = \delta_c q(\infty)/q(\infty) \tag{27b}$$

We may call z_j the input error of type j $(j = 1, 2, 3, 4)$, and y_i the output error in the ith layer $(i = 1, 2, 3)$.

(16), (19), and (22) are then written in the form

$$\sum_{i=1}^{3} a_{ki}\, y_i = \sum_{j=1}^{4} b_{kj}\, z_j \qquad (k = 1, 2, 3) \tag{28}$$

where

$$a_{1i} = x_i/m(\infty)$$

$$a_{2i} = x_i \int_{\Delta_i} p^{1+a_i}\, dh \Big/ \left[m(\infty)\, q(\infty) \int_{\Delta_i} p^{a_i}\, dh \right]$$

$$a_{3i} = x_i \int_{\Delta_i} G p^{a_i}\, dh \Big/ \left[E(\infty) \int_{\Delta_i} p^{a_i}\, dh \right] \tag{29}$$

$$\text{for } i = 1, 2, 3$$

and

$$b_{11} = b_{24} = b_{33} = 1$$

$$b_{12} = b_{13} = b_{14} = b_{23} = b_{31} = b_{34} = 0$$

$$b_{21} = R(\infty)/S(\infty)$$

$$b_{22} = A(\infty)/[S(\infty)m(\infty)\,q(\infty)]$$

$$b_{32} = -A(\infty)\,B(h_{10})/E(\infty) \qquad (30)$$

The set of equations (28) can be solved for y_i in terms of z_j; i.e.,

$$y_i = \sum_{j=1}^{4} c_{ij} z_j \qquad (i = 1, 2, 3) \qquad (31)$$

where the coefficient c_{ij} represents the sensitivity of the error of the ozone amount in the ith layer to the input error of the type j.

In order to examine the possible change in the sensitivity factors due to different modeling of δu, we consider in case A', below, that $\delta u(h)$ is represented by four connected straight-line segments. Assuming that $\delta u(h)$ is constant within the troposphere, zero at the 10 mb level, and arbitrary at the three connecting points--tropopause, 80 mb and 50 mb, we may reduce (16), (19), and (22) to the same form as (28) although the corresponding definition of coefficients a_{ki} is a little different from (29).

3.2 Numerical examples and discussion of the result

Since the sensitivity factor c_{ij} depends on the temperature and ozone distributions from which the coefficients in (28) are calculated, various combinations of these distributions should be examined so that a general conclusion may be obtained about the necessary degree of accuracy of the observations in order to secure a desired degree of

the determined ozone distributions. However, only a few numerical examples are shown below in which the assumed temperature and ozone distributions are rather typical. Since these examples disclose alarmingly large values of some of the sensitivity factors, further inclusion of a large number of examples is not essential to the purpose of this study.

The assumed distributions of ozone and temperature are shown in Fig. 3 , and their combinations for each case are given in Table 2 . Note that the difference between A and A' is in the difference in modeling δu as discussed above.

Table 2 . Combinations of ozone and temperature distributions in each case (see Fig. 3 for the distributions which are referred to by numbers).

Case	Ozone: u(h)	Tremperature	
		Troposphere	Stratosphere
A, A'	#1	#1	#1
B	#1	#2	#1
C	#2	#2	#1
D	#2	#2	#2

The final results of the sensitivity factors are summarized in Table 3. Note that a negative value of c_{ij} implies a reduced amount of ozone in the ith layer when the input error of type j is positive. As an example, consider Case A and suppose that there are no input errors except an error in the total amount of ozone (j = 1). If the observed total amount of ozone is larger by one percent than the true value, the amounts of ozone in the troposphere (i = 1) and in the lower stratospheric layer below the 50 mb level (i = 2) are underestimated, as seen from Table 3 , by 0.76 and 5.37 percent, respectively. On the other

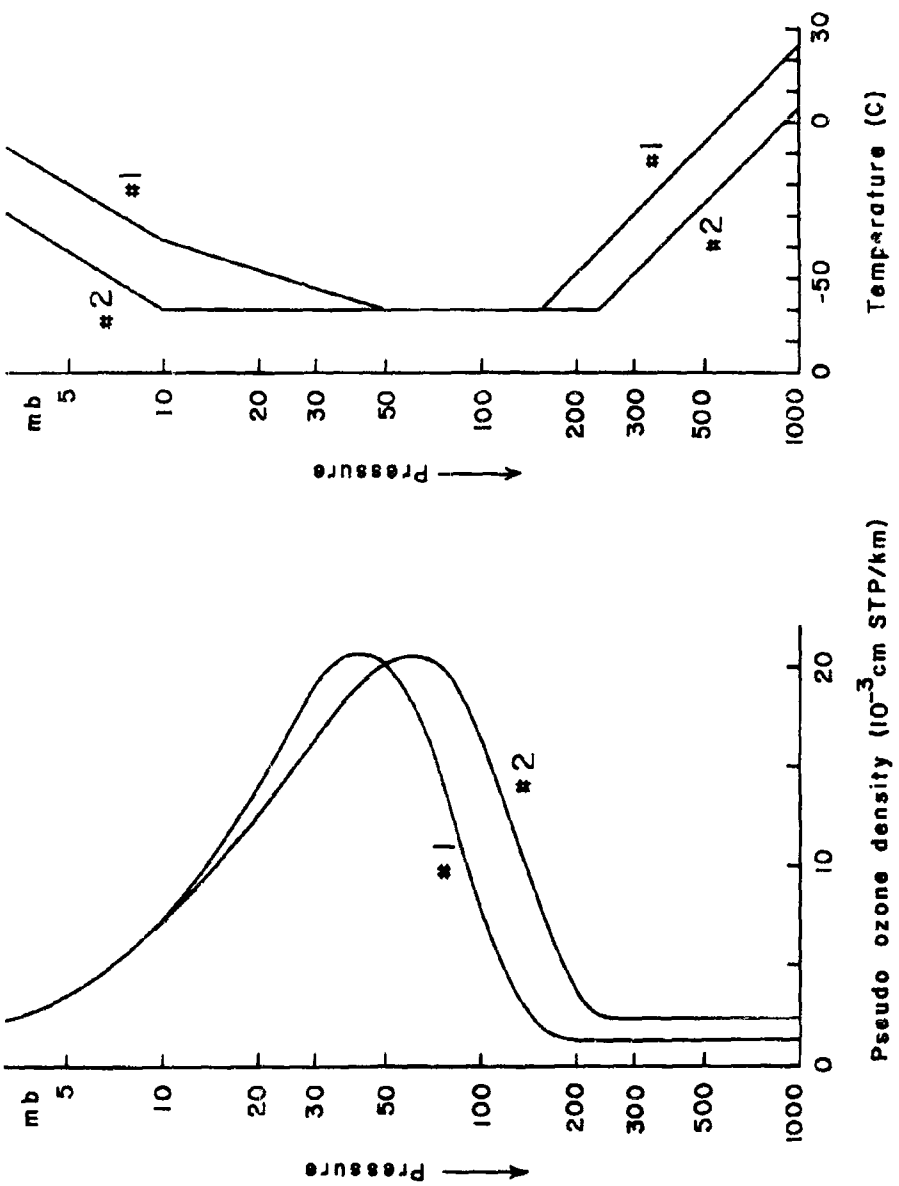

Figure 3. Various distributions of ozone (a) and temperature (b), assumed for the numerical examples. See Table 2 for their combination in each case.

hand, the ozone amount in the upper layer between 50 and 10 mb (i = 3) is overestimated by 4.41 percent. When the different types of input errors exist simultaneously, their contributions are algebraically additive.

Table 3 . Sensitivity factors, c_{ij}, in various cases.

i	Output error	Case	j = 1 $\frac{\delta m(\infty)}{m(\infty)}$	2 $\frac{\delta A(\infty)}{A(\infty)}$	3 $\frac{\delta E(\infty)}{E(\infty)}$	4 $\frac{\delta_c q(\infty)}{q(\infty)}$
1	$\frac{\delta x_1}{x_1}$	A	-0.76	- 0.52	3.25	0,86
		A'	-0.64	- 0.59	3.23	0.83
		B	-1.54	- 0.14	4.76	1.60
		C	-0.69	- 0.74	3.62	0.89
		D	0.00	- 3.00	4.02	0.00
2	$\frac{\delta x_2}{x_2}$	A	-5.37	18.27	-4.82	2.75
		A'	-4.41	15.68	-4.25	2.33
		B	-4.17	17.57	-7.07	1.62
		C	-4.29	16.08	-4.63	2.04
		D	-5.17	18.96	-5.14	3.17
3	$\frac{\delta x_3}{x_3}$	A	4.41	- 9.24	2.13	-1.48
		A'	3.91	- 7.91	1.84	-1.27
		B	3.88	- 8.92	3.13	-0.98
		C	6.18	-14.80	3.70	-2.04
		D	6.89	-17.10	4.11	-2.94

As seen in the rows of $\delta x_1/x_1$ in Table 3 , tropospheric ozone is distinctively sensitive to the error of emission intensity. Therefore, if the amount of tropospheric ozone is to be determined within an error of, say, 10 percent, the measurement of emission intensity must be accurate to within an error of at most 2 to 3 percent, while

the other types of input error may be larger than that. This finding agrees in general with Goody and Roach's (1956) contention that the infrared method (without simultaneous absorption measurement) is "capable of giving useful information about tropospheric ozone". However, there is the possibility as in Case D, that the accuracy of the absorption measurement is almost equally important in determination of the tropospheric ozone amount, although the assumed stratospheric temperature in this case is a little unusual.

For accuracy of the determined ozone amount in the second and third layers, the effect of the emission error remains at about the same relative level as for the tropospheric ozone, but sensitivity to the other types of input error is increased considerably. In particular, accurate absorption data are the decisive factors in obtaining reliable ozone distributions in the stratosphere.

If the ozone amounts in the two stratospheric layers are to be determined within an error of less than 10 percent, it can be seen from Table 3 that the error of the absorption data must be less than about 0.5 percent. Although the above error analysis has been made on the assumption that both the input and output errors are sufficiently small, the result may at least qualitatively be extended to a larger range of errors. Then, if the average error in the absorption measurements exceeds 5 percent, the stratospheric ozone distribution determined from such observational data will be almost totally valueless. Furthermore, since the absorption error affects the ozone amounts in the second and third layer in the opposite sense from each other, even a slight over or under correction of the raw absorption records for atmospheric water vapor could result in deceptive correlation

between the stratospheric ozone distribution and some other meteorological parameters.

Comparing the sensitivity factors for Case A' with those for Case A, we notice that their magnitudes are reduced, but only slightly, with use of the continuous model of $\delta u(h)$. It does not seem likely that a substantial reduction of sensitivity can be achieved by proper choice of a model, although some models may prove less sensitive than others.

Considering the infrared method as a means of determining stratospheric ozone distributions, we now recognize that rigorous care must be taken to reduce the magnitude of the input errors. Since there is no standardized way of obtaining the absorption and emission data as in the case of the total amount of ozone, assessment of errors of these observational data has to be made with specific instrumentation and with specific procedures through which raw observational records are transformed into numerical values and also corrected for influences of water vapor, carbon dioxide, etc. Discussion of these technical details, however, is beyond the scope of this paper.

An estimate of the fourth type error, which is caused by the use of the inverted Curtis-Godson approximation, is given in the following section. A likely value of $\delta_c q(\infty)/q(\infty)$ is found to be about minus 20 to 30 percent, although it depends on the vertical ozone distribution and the air mass in the direction of observation. If the values of sensitivity factors in Table 3 are used, then it is found that this error alone would rather consistently result in underestimation of the ozone amounts in the first and second layers by about 20 and 50 percent, respectively, and in overestimation of the ozone amount in the third layer by about 40 percent. Thus, some kind of correction for this type of input error must

be devised. A crude way of eliminating a gross systematic error in the mean pressure is to increase the observed spectroscopic mean pressure by adding a constant amount or multiplying by a constant factor for all observations. A flat increase of 10 mb, which Goody and Roach (1956) adopted for practical reasons, may be justified because such a procedure should have reduced a large portion of the systematic error in the tropospheric ozone amount. However, a more refined method of correction should be developed for determination of the stratospheric ozone distribution because of the higher sensitivity there.

4. On the inverted Curtis-Godson approximation

4.1 The case of a single Lorentz line

As mentioned previously in Section 2, the Curtis-Godson approximation in the original form is to estimate the absorption due to an absorbing gas which is distributed with different pressure along the path of radiation. This is achieved by considering a path with the same amount of the absorbing gas at a uniform pressure which is equal to the mean pressure of the mass distribution of the absorbing gas on the original variable-pressure path. However, in the infrared method of determining the vertical distribution of the atmospheric ozone, it is necessary to estimate the mean pressure of the ozone distribution from the observed absorption along a variable-pressure path. A simple method of doing this is to use the Curtis-Godson approximation in an inverted way; that is, the mean pressure is taken to be equal to the spectroscopic mean pressure, the latter being defined as the pressure at which a uniform-pressure path with an equal amount of the absorbing gas would give exactly the same absorption as observed along the variable-pressure path.

Unfortunately, however, the accuracy of the inverted approximation is not as good as one might expect from the favorably checked accuracy of the original approximation. We shall first demonstrate this for the absorption due to a single Lorentz line. The extreme simplification of spectrum has to be made for mathematical expediency. An extension of the result to the absorption due to the 9.6μ ozone band will be shown later in this section.

The absorption coefficient, $k(\nu, p)$, of a Lorentz line is given by

$$k(\nu, p) = \frac{S}{\pi} \frac{a}{\nu^2 + a^2} \tag{32}$$

where S is the line intensity, ν is the distance from the line center on the wave number scale, and a is the half width of the line, which is assumed as usual to be proportional to the pressure, p, so that if a_o is the half width at a standard pressure p_o,

$$a = a_o(p/p_o) \quad .$$

Consider a distribution of absorbing gas with respect to pressure, which may be represented by the cumulative distribution function m(p) along a path. The integrated absorptivity (the equivalent width) due to the entire path is a functional of the distribution function m(p) and is given by the integral

$$A[m(p)] = \int_{-\infty}^{\infty} \left\{1 - \exp\left(-\int_o^M k(\nu, p)dm\right)\right\} d\nu \tag{33}$$

where M is the total mass (per unit cross section) of absorbing gas along the path and p in the integrand is considered implicitly as a function of m.

In the assumed case of a single Lorentz line, we may write

$$A[m(p)] = 2\int_0^\infty \{1 - \exp(-2\gamma N(\nu))\}\, d\nu \tag{34}$$

where

$$\gamma = SM/(2\pi a_o)$$

and

$$N(\nu) = \int_0^1 \frac{2(p/p_o)}{(\nu/a)^2 + 1}\, d(m/M)$$

We may consider a special case in which the whole mass of the absorbing gas is at a certain pressure p, i.e., the case of uniform pressure path. The integrated absorptivity of such a path is a function of M and p, and it is denoted specifically by $\bar{A}(M, p)$. Integral (34) for a uniform pressure path can be expressed in terms of Bessel functions (after Ladenburg and Reiche; see Elsasser, 1942), namely

$$\bar{A}(M, p) = 2\pi a_o r f(\gamma/r) \tag{35}$$

where

$$r = p/p_o$$

and the function f(x) is defined by

$$f(x) = xe^{-x}(J_o(ix) - iJ_1(ix))$$

whose numerical values are listed in the paper by Elsasser. It is easily shown that, for large values of γ,

$$\bar{A}(M, p) \sim 2a_o(2\pi\gamma r)^{1/2} \tag{36}$$

and for small values of γ,

$$\bar{A}(M, p) = 2a_o\pi\gamma[1 - \gamma/(2r) + \cdots] \tag{37}$$

Integral (34) is generally impossible to solve in a closed form for an arbitrary distribution m(p). The only exception is the case where m(p) is a linear function of p; that is, where the mixing ratio of the absorbing gas to the air is constant through a layer. When such a layer has a finite thickness, the integral (34) may be expressed in terms of a hypergeometric function (Strong and Plass, 1950). In particular, for an infinite layer extending from the ground at pressure p_o to $p = 0$, the cumulative distribution function with a constant mixing ratio is written

$$m(p) = (p_o - p)M/p_o = (1 - r)M \tag{38}$$

and the integrated absorptivity is given by

$$A[m(p)] = 2a_o\pi^{\frac{1}{2}}\Gamma(\gamma + \tfrac{1}{2})/\Gamma(\gamma) \tag{39}$$

The limiting values are, for large values of γ,

$$A[m(p)] \sim 2a_o(\pi\gamma)^{\frac{1}{2}} \tag{40}$$

and for small values of γ,

$$A[m(p)] = 2a_o\pi\gamma[1 - (2\ln 2)\gamma + \cdots] \tag{41}$$

The spectroscopic mean pressure, q_s, as defined previously, is determined from

$$\bar{A}(M, q_s) = A[m(p)]$$

or

$$2a_o\pi r_s f(\gamma/r_s) = 2a_o\pi^{\frac{1}{2}}\Gamma(\gamma + \tfrac{1}{2})/\Gamma(\gamma) \tag{42}$$

where

$$r_s = q_s/p_o \ .$$

The limiting values of q_s are explicitly determined by making use of (36) and (40), or (37) and (41); i.e.,

$$q_s \to p_o/2 \text{ as } \gamma \to \infty$$

and

$$q_s \to p_o/(4 \ln 2) = 0.361\, p_o \quad \text{as} \quad \gamma \to \infty .$$

The mean pressure, q, of the mass distribution (38) in this example is

$$q = \int_o^M p\, dm/M = p_o/2 .$$

Thus, the inverted Curtis-Godson approximation of estimating the mean pressure from the spectroscopic mean pressure is asymptotically correct only for large values of γ. At the other extreme end of $\gamma \to 0$, the spectroscopic mean pressure is about 30 percent smaller than the mean pressure. The ratio q_s/q for intermediate values of γ is shown by the top curve in Figure 4.

It may be shown, on the other hand, that the original Curtis-Godson approximation of estimating the absorption along a variable-pressure path is exact in the two limiting cases of $\gamma = 0$ and $\gamma \to \infty$, while, for intermediate values of γ, the approximation overestimates the absorption. In the above example of a path with a constant mixing ratio, however, the error does not exceed 6 percent.

As the second example, we take another kind of simple distribution in which the density of the absorbing gas is constant throughout a layer between the ground at $p_o = 1000$ mb and at a top level at $p_1 = 10$ mb. Since the effect of temperature variation with height on the air density is rather small in the atmosphere, the mixing ratio of the absorbing gas may be assumed to be inversely proportional to the air pressure. Then the cumulative distribution function is given by

$$m(p) = M \ln(p_o/p)/\ln(p_o/p_1) \tag{43}$$

and the mean pressure of this distribution for the entire layer is

$$q = (p_o - p_1)/\ln(p_o/p_1)$$
$$= 215 \text{ mb}$$

The spectroscopic mean pressure is determined in the same way as in the first example, but entirely by numerical computation. The result, as the ratio q_s/q, is shown by the bottom curve in Figure 4. The ratio in the limit as $\gamma \to 0$ is about 0.35.

The distributions that have been considered in the above examples do not correspond to any typical distribution of the atmospheric ozone. The latter has a principal maximum of density somewhere between the 100 mb and 10 mb levels, and the density in the troposphere is smaller than the maximum by about one order of magnitude. Therefore, a major part of the atmospheric ozone concentrates in a smaller range of pressure variation than that given by the constant density distribution in the second example. In this sense, the bottom curve in Figure 4 may safely be considered to present a lower bound to the ratio q_s/q which may be found for an actual ozone distribution. On the other hand, the top curve, corresponding to a distribution with constant mixing ratio (i.e., exponential decrease in density), may present an upper bound.

As the last example (still assuming a single Lorentz line), we consider a distribution that is similar to that of atmospheric ozone. In order to simplify the computation, a continuous distribution with respect to pressure is replaced by the superposition of four uniform-pressure paths at different pressures. The assumed numerical values in the

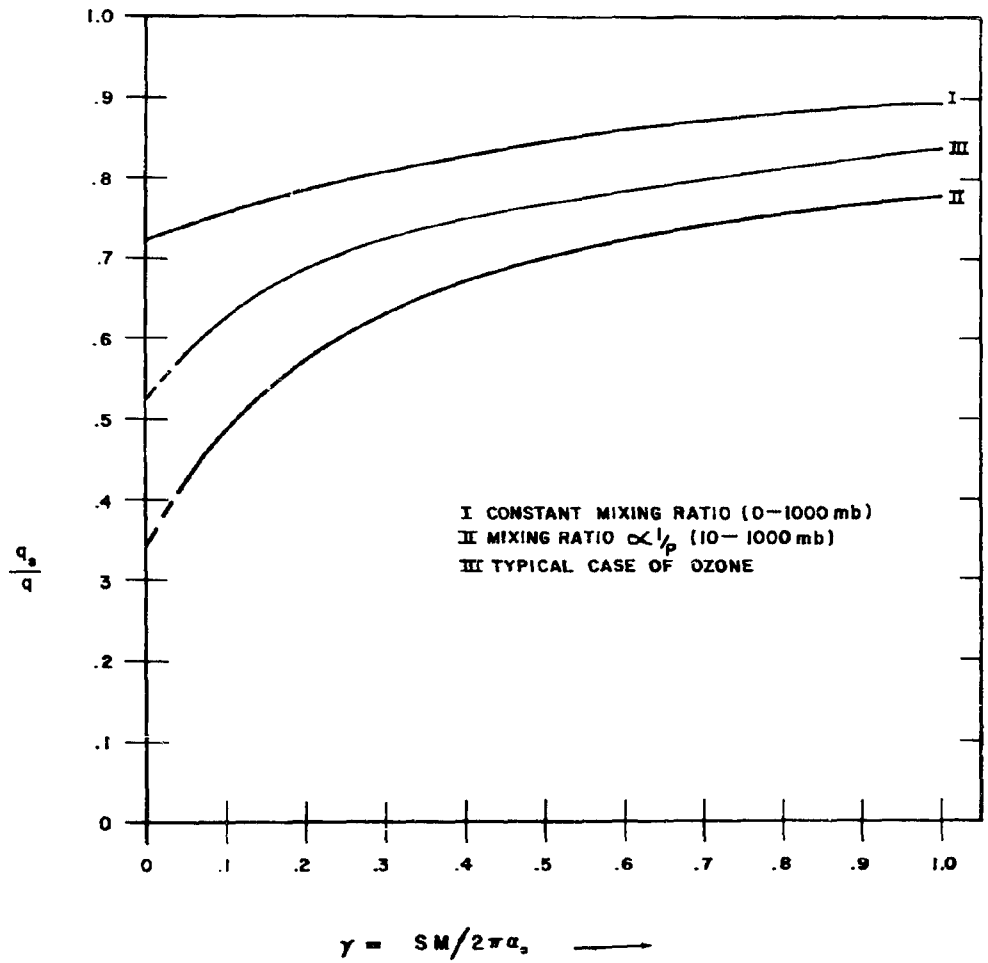

Figure 4. The ratio of the spectroscopic mean pressure to the mean pressure of the mass distribution of an absorber, q_s/q, computed for a single Lorentz line.

computation are shown in Table 4

Table 4. Assumed ozone distribution

Layer	Pressure	Amount of ozone relative to the total (M)
1	503 mb	5.5%
2	108	27.4
3	25	54.8
4	5.7	12.3

The mean pressure of this distribution is

$$q = 7.3 \text{ mb} .$$

The spectroscopic mean pressure is shown again as the ratio q_s/q in Figure 4 .

4.2 Application to the case of the 9.6μ band

It is too laborious, if not impossible, to compute an integral like (3) with the actual spectrum of the 9.6μ band of ozone. If the intensity and half width of all lines in the band are identical but the line centers are located at random, a simple statistical model of band absorption may be applied to the computation. It is shown in such a case (Kaplan, 1953; Godson, 1955) that the essential problem in evaluating the integral is reduced to that of the case of a single isolated line. However, when we consider the 9.6μ ozone band as a whole, such a simple statistical model seems hardly to be applicable. Nevertheless, if we try to extend the above result to the ozone problem, it is necessary to have at least an estimate of the order of magnitude of γ, which might be characteristic of the absorption due to the ozone band, because the whole consideration in this section would become unnecessary if such a characteristic value of γ were found to be very large.

The line intensity distribution in the 9.6μ band, taken from

the theoretical computation by Filler (1951) agrees well with the logarithmic ogive which is considered by Godson (1955) in his statistical model. The empirical curves of the absorption band area of the 9.6μ band (Fig. 1) are found to fit fairly well in a range of the ozone amount less than 0.4 cm STP to the theoretical curves due to the Godson model, if values of the two parameters in the model are properly chosen at each pressure for the curve to be fitted. From the two values of the parameters at each pressure, we may determine a kind of mean line intensity. (Specifically, it is an empirical value for $(\Sigma S_t / \Sigma S_t^{\frac{1}{2}} a_{o_t}^{\frac{1}{2}})^2 / 2\pi$ which is a generalization of $S/2\pi a_o$ in the simpler statistical model with constant line intensity and half width. The subscript t is to identify individual lines and the summation is to be taken over all the lines in the band.) The values of $S/2\pi a_o$ which are thus determined to represent the 9.6μ band are shown in Table 5 .

Table 5. $S/2\pi a_o$ for the 9.6μ band

p (mb)	20	100	400
$S/2\pi a_o$ (cm STP)$^{-1}$	0.44	0.69	1.38

The dependency on the pressure at which curves are fitted, and the fact that a good fit between the empirical curves and the theoretical is not obtainable for the ozone amount greater than 0.4 cm STP are probably because the assumption of the random line distribution in the statistical model is not fulfilled in the actual ozone band. Thus, some ambiguity still remains in just what value of $S/2\pi a_o$ should be taken for a variable-pressure path, although the order of magnitude is fairly well established.

In the last example of numerical computation of the spectro-

scopic mean pressure, the mean pressure of the distribution is 71.3 mb. We may take

$$S/2\pi a_o = 0.6 \text{ (cm STP)}^{-1}$$

as a rough but reasonable value, in order to make correspondence between the single line model and the 9.6μ band. Then, if the total amount of ozone in a vertical column is 0.3 cm STP, the spectroscopic mean pressure for various air mass , at which the absorption measurement is made, is obtained as shown in Table 6 .

Table 6. Spectroscopic mean pressure for the ozone distribution given in Table

Air mass	1	1.5	2	3	5	∞
M (cm STP)	0.3	0.45	0.6	0.9	1.5	∞
γ	.18	.24	.36	.54	.90	∞
q_s/q	.65	.70	.73	.77	.83	1.00
q_s (mb)	46.3	49.9	52.0	54.9	59.2	71.3

The above numerical result is derived only for a particular case of the ozone distribution under crude assumptions. However, it seems to be evident that the use of the inverted Curtis-Godson approximation seriously underestimates the mean pressure, possibly by about 20 to 30 percent. Implication of this error in the infrared method of determining the vertical ozone distribution was already discussed in preceding sections.

5. Conclusion

The infrared method as described in Section 2 can provide us with a broad profile of the vertical distribution of atmospheric ozone from the observations with optical instruments at a ground station, of the total ozone amount, the integrated absorptivity of the 9.6μ ozone

band in the direct solar beam and the ozone emission intensity in the same band. However, the determined ozone distribution is found to be very sensitive to errors in the observations. If the ozone amount in each layer of the two stratospheric layers is to be accurate to an error of less than 10 percent, for instance, the error in the absorption measurement (including its correction for effects of other gases) must be less than about 0.5 percent. It is also found that the use of the inverted Curtis-Godson approximation leads to a considerable amount of systematic error in the determined ozone distribution, its magnitude reaching, for instance, 50 percent in the lower stratospheric layer.

The question as to how accurate the determined ozone distribution should be depends, of course, on intended use of the results. For the purpose of quantitative estimation of the stratospheric motion with the use of ozone as a tracer, an error of more than 5 percent in the determined ozone density is perhaps not acceptable. On the other hand, for the purpose of inferring a large scale pattern of the stratospheric circulation or studying the correlation between the ozone distribution and tropospheric meteorological parameters based on monthly or seasonal statistics, a purely random error of 10 or even 20 percent in the determination of the individual ozone distribution might be tolerated. Even if this were the case, however, one would have to eliminate scrupulously any systematic error in the observation data which is correlated to atmospheric conditions.

Acknowledgments

The writer is greatly indebted to Prof. A. Adel of Arizona State College for discussions of the infrared observation and for the borrowed observation records; and to Dr. C. D. Walshaw of the University of Cambridge for the copy of complete data of his laboratory measurements. The writer also wishes to express his appreciation to Prof. J. London for his advice and encouragement.

References

Brewer, A. W., et al, 1960: Distribution verticale de l'ozone atmosphérique. Comparison de diverses méthodes. Annales de Geophysique, 16, 196-222.

Curtis, A. R., 1952: Discussion of Goody's "A statistical model for water-vapor absorption". Quart. J. R. Meteor. Soc., 78, 638-640.

Elsasser, W. M., 1942: Heat transfer by infrared radiation in the atmosphere. Harvard Meteor. Studies, No. 6, 107 pp.

Epstein, E. S., 1957: VODARO computing methods. Technical Memorandum to the Director, GRD. GRD-TM-57-15, 17 pp.

Epstein, E. S., C. Osterberg, and A. Adel, 1956: A new method for the determination of the vertical distribution of ozone from a ground station. J. Meteor., 13, 319-334.

Filler, A. S., 1951: The structure of the 9.6 micron band of ozone. Stratospheric Radiation Tech. Rep. No. 2, Univ. of Utah.

Godson, W. L., 1955: The computation of infrared transmission by atmospheric water vapor. J. Meteor., 12, 272-284.

Goody, R. M., and W. T. Roach, 1956: Determination of the vertical distribution of ozone from emission spectra. Quart. J. R. Meteor. Soc., 82, 217-221.

Goody, R. M., and W. T. Roach, 1958: The determination of tropospheric ozone from infra-red emission spectra. Quart. J. R. Meteor. Soc., 84, 108-117.

International Ozone Commission, 1956: Report of Conference of Infra-Red Panel. (Unpublished.)

Kaplan, L. D., 1953: A quasi-statistical approach to the calculation of atmospheric transmission. Proc. Toronto Meteor. Conference, 43-48.

Strong, J., and G. N. Plass, 1950: The effect of pressure broadening of spectral lines on atmospheric temperature. Astrophys. J., 112, 365-379.

Summerfield, M., 1941: I. The effect of pressure on the infra-red absorption of ozone, and II. An ultra-spectrometer technique for infra-red bands. Doctoral thesis, California Institute of Technology, 88 pp.

Vigroux, E., 1959: Distribution verticale de l'ozone atmosphérique d'après les observations de la band 9.6μ. Annales de Geophysique, 15, 516-538.

Walshaw, C. D., 1957: Integrated absorption by the 9.6μ band of ozone. Quart. J. R. Meteor. Soc., 83, 315-321.

Walshaw, C. D., 1960: The accuracy of determination of the vertical distribution of atmospheric ozone from emission spectrophotometry in the 1,043 cm^{-1} band at high resolution. Quart. J. R. Meteor. Soc., 86, 519-529.

PART II

Absorption Processes in the Stratosphere and Mesosphere

by

J. London and C. Prabhakara

1. Introduction

It has become increasingly recognized that atmozpheric ozone plays a dual, and in both cases important, role in the dynamics and energetics of the upper atmosphere. Because of its relatively long life below 30 km (which includes the region of maximum concentration) ozone participates in the general circulation of the upper troposphere and lower stratosphere in a very direct sense. As a result, studies of the ozone budget are closely linked to an understanding of circulation processes in this region of the atmosphere. Also, because ozone absorbs solar ultraviolet radiation very strongly, it contributes to the energy sources and subsequent temperature structure of the region from 20-80 km.

The absorption of solar radiation in the stratosphere and mesosphere is due almost completely to the strong absorption by ozone in the spectral region $\lambda \leq 3200\,\text{Å}$. The net result of this absorption of solar energy is first to produce a quasi-stable distribution of ozone and then, through ozone absorption in the strong Hartley bands, to produce the temperature maximum at the stratopause (about 50 km). The following discussion describes calculations of the photochemical equilibrium distribution of ozone as a function of height, latitude and season; and the subsequent absorption of solar radiation in the stratosphere and mesosphere assuming the computed ozone distributions obtain. Some of the limitations of the results are also discussed.

2. The photochemical distribution of ozone

The first complete theory for the presence and distribution of ozone in the upper atmosphere was given by Chapman (1930). Since that time extensions to both theory and calculations have been made by Wulf and Deming (1936), Craig (1950), Dütsch (1956), and others. According to the theory, the presence of atmospheric ozone results from a combination of processes involving photodissociation and recombination. Ozone is formed mainly by photodissociation of molecular oxygen and then recombination between atomic and molecular oxygen. Ozone is then destroyed directly by photodissociation and by recombination with atomic oxygen. The chief photochemical reactions involving the formation and destruction of ozone are assumed to be

$$O_2 + h\nu \rightarrow O + O \tag{1}$$

$$O + O + M \xrightarrow{k_1} O_2 + M \tag{2}$$

$$O + O_2 + M \xrightarrow{k_2} O_3 + M \tag{3}$$

$$O_3 + h\nu \rightarrow O_2 + O \tag{4}$$

$$O + O_3 \xrightarrow{k_3} 2O_2 \tag{5}$$

$h\nu$ represents the photo energy necessary to dissociate molecular oxygen or ozone; k_1, k_2, k_3 are the reaction rate coefficients describing processes (2), (3), and (5); and M represents any third body in the three-body collison described in Eqs (2, 3). The presence of M is necessary in order to preserve the total energy and momentum of the colliding particles in the system.

If we assume that equilibrium among these five reactions obtains,

we can write two equations

$$\frac{dn_1}{dt} = 2f_2 n_2 + f_3 n_3 - 2k_1 n_1^2 n - k_2 n_1 n_2 n - k_3 n_1 n_3 = 0 \tag{6}$$

and

$$\frac{dn_3}{dt} = -f_3 n_3 + k_2 n_1 n_2 n - k_3 n_1 n_3 = 0 \tag{7}$$

where n, n_1, n_2, n_3 are the number density of air molecules, atomic oxygen, molecular oxygen, and ozone respectively; and f_2, f_3 are the number of quanta of solar radiation absorbed per molecule per unit time.

$$f_2 = \int_\lambda \sigma_2 q_\lambda \, d\lambda = \int_\lambda \sigma_2 q_{\infty\lambda} \exp(-\sigma_2 N_2 - \sigma_3 N_3) \, d\lambda \tag{8a}$$

$$f_3 = \int_\lambda \sigma_3 q_\lambda \, d\lambda = \int_\lambda \sigma_3 q_{\infty\lambda} \exp(-\sigma_2 N_2 - \sigma_3 N_3) \, d\lambda \tag{8b}$$

where σ_2, σ_3 are the absorption cross sections of O_2 and O_3; $q_{\infty\lambda}$ represents the number of quanta $cm^{-2} sec^{-1}$ per unit wavelength in the solar beam available at the top of the atmosphere; N_2 and N_3 represent the total number of oxygen or ozone molecules above some level and in the direction of the solar beam.

The equilibrium conditions described in (6) and (7) can be solved to give

$$n_3 = n_2 \left[\frac{(f_2/f_3) k n \cdot n_2 (1 - x)^2}{f_3 (k_1/k_2 k_3) + n_2 (1 - x)} \right]^{\frac{1}{2}} \tag{9}$$

where $k = k_2/k_3$ and $x = (n_3/k n \cdot n_2)$.

Since any atmospheric gas can act as the third body in reactions (2) and (3), N_2 (nitrogen) and O_2 will be the third body 99 percent of the time except at levels above 80 km where the number of oxygen atoms becomes quite large. The relative efficiencies of N_2 and O_2 acting as

third bodies in the collision processes described by Eqs (2, 3) are not very well known, and we will assume that both gases are equally efficient. For a mixed, dry atmosphere, the number of nitrogen molecules is equal to $3.76\,n_2$ and $k_n \cdot n_2 = k_{n_2}(4.76)\,n_2$.

Thus

$$n_3 = 2.25\,n_2^2\left[\frac{(f_2/f_3)\,k(1-x)^2}{f_3(k_1/k_2k_3) + n_2(1-x)}\right]^{\frac{1}{2}} \tag{10}$$

In order to simplify this relationship further, it is convenient to evaluate the order of magnitude of the various terms and to make suitable approximations. The orders of magnitude given in the table below represent average values of the parameters in Eq (10). The references for these values are discussed below.

We see that for all levels $x \lesssim 10^{-2} \ll 1$ and we can write

$$n_3 = 2.25\,n_2^2\left[\frac{(f_2/f_3)\,k}{f_3(k_1/k_2k_3) + n_2}\right]^{\frac{1}{2}} \tag{11}$$

Also, at levels below about 50 km, the first term in the denominator is smaller than the second term by a factor of at least 100. Therefore, for levels below 50 km, we have

$$n_3 = 2.25\,n_2[f_2/f_3(k)n_2]^{\frac{1}{2}} \tag{12}$$

This equation is the same as that given by Dütsch (1956).

According to Eq (12) the equilibrium ozone concentration below 50 km depends on the solar ultraviolet ratio f_2/f_3 and the recombination ratio, k. Changes in n_3 would require changes in the relative values of f_2 as compared to f_3. The role of the recombination rate ratio k is to stabilize the ozone production in the region below 50 km. If we regard Eqs (1 - 5) as the primary reactions for determining the photochemical

Table 1. Approximate values for the parameters in the photochemical equations.

ht	T	n_2	f_2	n_3	f_3	k_1	k_2	k_3	x	$\frac{f_3 k_1}{k_2 k_3}$
km	°K	/cm^3	quanta/sec^1	/cm^3	quanta/sec	cm^6/molec^2/sec	cm^6/molec^2/sec	cm^3/molec/sec		
80	190	8×10^{13}	4×10^{-9}	5×10^{8}	1×10^{-2}	7×10^{-33}	3×10^{-34}	1×10^{-16}	5×10^{-3}	2×10^{15}
70	220	4×10^{14}	2×10^{-9}	2×10^{9}	1×10^{-2}	7×10^{-33}	3×10^{-34}	5×10^{-16}	5×10^{-3}	5×10^{14}
60	255	1×10^{15}	1×10^{-9}	1×10^{10}	1×10^{-2}	8×10^{-33}	3×10^{-34}	2×10^{-15}	1.5×10^{-2}	1×10^{14}
50	280	5×10^{15}	7×10^{-10}	5×10^{10}	5×10^{-3}	8×10^{-33}	3×10^{-34}	5×10^{-15}	8×10^{-3}	3×10^{13}
40	265	1×10^{16}	5×10^{-10}	5×10^{11}	1×10^{-3}	8×10^{-33}	3×10^{-34}	3×10^{-15}	1.5×10^{-2}	10^{13}

equilibrium distribution of ozone, we require the following data to compute n_3 from Eq (11) or Eq (12).

(a) $q_{\infty\lambda}$ -- the spectral distribution (in absolute intensities of the solar beam at the top of the atmosphere for wavelengths covering the interval of O_2 and O_3 absorption in the ultraviolet and visible. For purposes of the present computation, this includes the region 1700 Å to 7500 Å.

(b) σ_2, σ_3 -- the absorption cross sections of O_2 and O_3 in this spectral interval.

(c) k_1, k_2, k_3 -- the reaction rate coefficients appropriate to Equations (2), (3), and (5).

(d) The distribution of temperature and pressure and the resulting distribution of n_2 in the atmosphere (20 - 80 km).

2.1 The spectral distribution of solar radiation

The solar radiation curve approximates an equivalent black body radiator (of about 6000°K) in the visible and near infrared part of the spectrum. Because of the strong absorption by ozone it was impossible in earlier years to obtain solar spectra that extended below about 2800 Å. Rocket observations taken since 1946, however, have extended the observed spectrum down to 2200 Å and in some cases through sections of the far ultraviolet. The origin of the solar spectrum in the interval 1500 Å - 2000 Å is not clearly understood and there has been some speculation of the character of the solar emission curve for this region. The observations show that the solar spectral curve in the region 3000 Å to 2000 Å falls off sharply to an equivalent black body curve of about 5000°K.

The energy spectrum used in the present calculations were taken

from Johnson (1954), and Johnson et al (1954) who used the available observations to reconstruct a solar energy curve for the range 2200 Å to 8000 Å. We then extrapolated these values to fit an equivalent black body curve of 5000°K at 2000 Å to 4500°K in the wavelength region 1900 Å to 1700 Å.

After the calculations for n_3 were completed, additional rocket spectra became available (Detwiler et al, 1961) indicating that the intensity distribution in the solar ultraviolet at 1750 Å corresponds to an equivalent black body radiating temperature of about 4700°K. Since the equilibrium concentration of ozone below 50 km is given by $n_3 \alpha (f_2/f_3)^{\frac{1}{2}}$ an increase in the value of f_2 (holding f_3 constant) will increase the ozone concentration. This correction should apply to the ozone distribution at the levels 40-50 km where radiation in the interval 1900-2000 Å is most effective as will be shown below.

2.2 Absorption cross sections for O_2 and O_3

1. Oxygen: There are three important regions in the ultraviolet for absorption by molecular oxygen. These are

   a. Schumann-Runge continuum (1250 Å - 1750 Å). This region is largely responsible for the dissociation of oxygen above 80 km.

   b. Schumann-Runge bands (1751 Å - 2026 Å). These bands are absorbed in the mesosphere principally in the layer 50-80 km.

   c. Herzberg continuum ($\lambda < 2424$ Å). Although absorption in this region represents the weakest of the three, absorption in the spectral interval 2000 Å - 2200 Å

is responsible for the major production of ozone in the stratosphere and mesosphere. Solar radiation at 2000 Å - 2200 Å penetrates deeply into the stratosphere resulting in dissociation of molecular oxygen at a level where the chance for three body recombination to form ozone is quite good.

The oxygen absorption cross sections used in Eq (8a) for the interval 1700 Å - 1950 Å were taken from Watanabe (1958). For the interval 2100 Å - 2424 Å it was assumed that the oxygen absorption was pressure dependent in the manner discussed by Götz (1951). The absorption cross sections were approximated for zero pressure from the values given by Götz. For the spectral region 1950 Å - 2100 Å the values were extrapolated between the data as discussed above.

2. Ozone: The important regions for ozone absorption are the weak Chappuis bands in the visible spectrum, the Huggins bands, and the contiguous Hartley bands. Of these three, Hartley absorption is by far the most important. Although the ozone absorption cross section for $\lambda < 2020$ Å increases again, this increase is in a region of decreasing solar energy and represents only a minor contribution to the absorption process in the stratosphere and mesosphere. The absorption cross sections for ozone were taken from Vigroux (1953) for wavelengths larger than

2300 Å and from Inn and Tanaka (1953) and Watanabe (1958) for the region below 2300 Å. These values represent the results of careful laboratory experiments and are probably the most reliable available at the present time.

The distribution of solar radiation at the top of the atmosphere ($q_{\infty\lambda}$) and absorption cross sections (σ_2, σ_3) used in the present calculations are given in Figs. 1(a), 1(b). Curves (1) and (2) of Fig. 1(a) refer to the absorption cross sections of ozone and molecular oxygen ($cm^2 molec^{-1}$). Curve (3) refers to the solar energy arriving at the top of the atmosphere on a surface perpendicular to the sun's rays (units of right hand coordinate are quanta $cm^{-2} sec^{-1} Å^{-1}$). Fig. 1(b) shows the absorption cross section for ozone [curve (1)] and the solar energy distribution [curve (2)] on a compressed wavelength scale.

2.3 The rate reaction coefficients

The recombination rate coefficients k_2 and k_3 were taken from recent re-analysis by Campbell and Nudelman (1960) of the data of Glissmann and Schumacher. They give as best estimates for the individual rate coefficients for the reaction given by Eqs (3, 5):

$$k_2' = 1.87 \times 10^{14} \exp[149/T]\, cm^6/gm\ mol^2/sec$$

$$k_3 = 5.44 \times 10^{12} \exp[-2133/T]\, cm^3/gm\ mol/sec$$

where the third body in the reaction for k_2' was O_3. Campbell and Nudelman assume that the efficiency of k_2' is reduced by one-third when the third body in Eq (3) is O_2 (or presumably N_2). Therefore, we can write for the reaction rate ratio for the atmosphere:

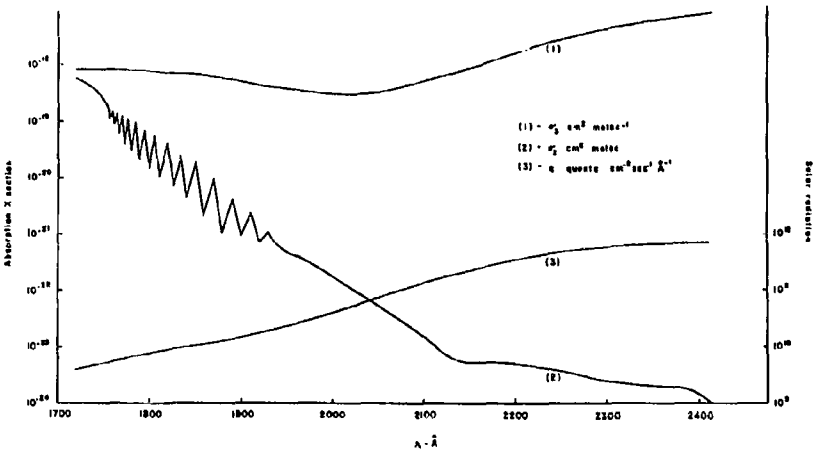

Fig. 1(a) The spectral distribution of absorption cross section ($cm^2\,molec^{-1}$) for ozone and oxygen, and solar ratiation (quanta $cm^{-2}\,sec^{-1}\,Å^{-1}$) received at the top of the atmosphere on a surface perpendicular to the sun's rays. Spectral interval 1700 Å - 2424 Å.

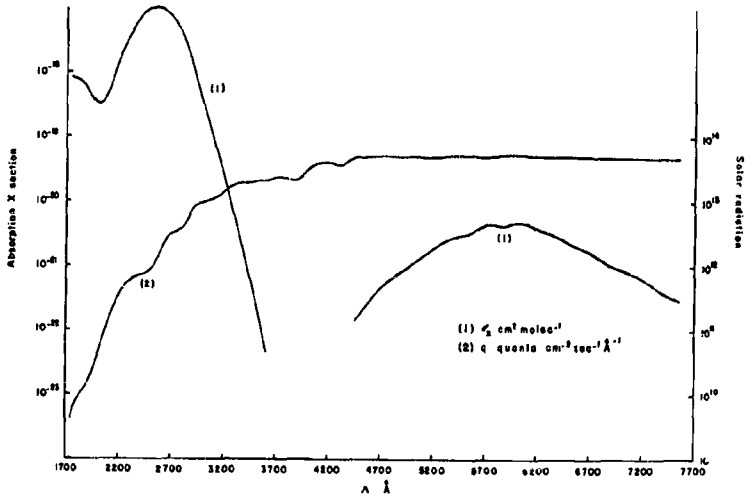

Fig. 1(b) The same for ozone and solar radiation. Spectral interval 1700 Å - 7500 Å.

$$k = \frac{k_4'}{3k_3} = 1.9 \times 10^{-23} \exp(2282/T)\ \text{cm}^3/\text{molecule}. \qquad (13)$$

The estimate of k thus derived can be compared with earlier values as given by Eucken and Patat (1936) for the range of temperatures observed in the stratosphere and mesosphere. It is seen from Fig. 2 that the two curves are quite close in the region of relatively low temperatures (~200°K) and differ only by a factor of 2 at temperatures corresponding to the stratopause (~290°K). As will be indicated below, however, variations in k are important only at the level of the mesopause where the self-regulating mechanism on ozone formation is weakened. It is in this region that the difference between the two curves shown in Fig. 2 is quite small.

The equilibrium distribution of ozone at levels above about 60 km depends on the values for the rate coefficients used in Eq (11). Since both k_1 and k_2 describe three body recombination processes, the ratio of their values has been taken as independent of temperature. It is clear from Eq (11) that as the ratio k_1/k_2 increases, the equilibrium value for ozone will decrease. The value used for the rate ratio in the present computations was $k_1/k_2 = 1.5$. This value is somewhat low when compared to the ratio of the individual rate coefficients given by Bates and Nicolet (1950) and Campbell and Nudelman (1960) as shown in Table 1 above. The use of the larger rate ratio would not affect the equilibrium ozone concentration below 65 km but would reduce the values above 75 km by about 60 percent.

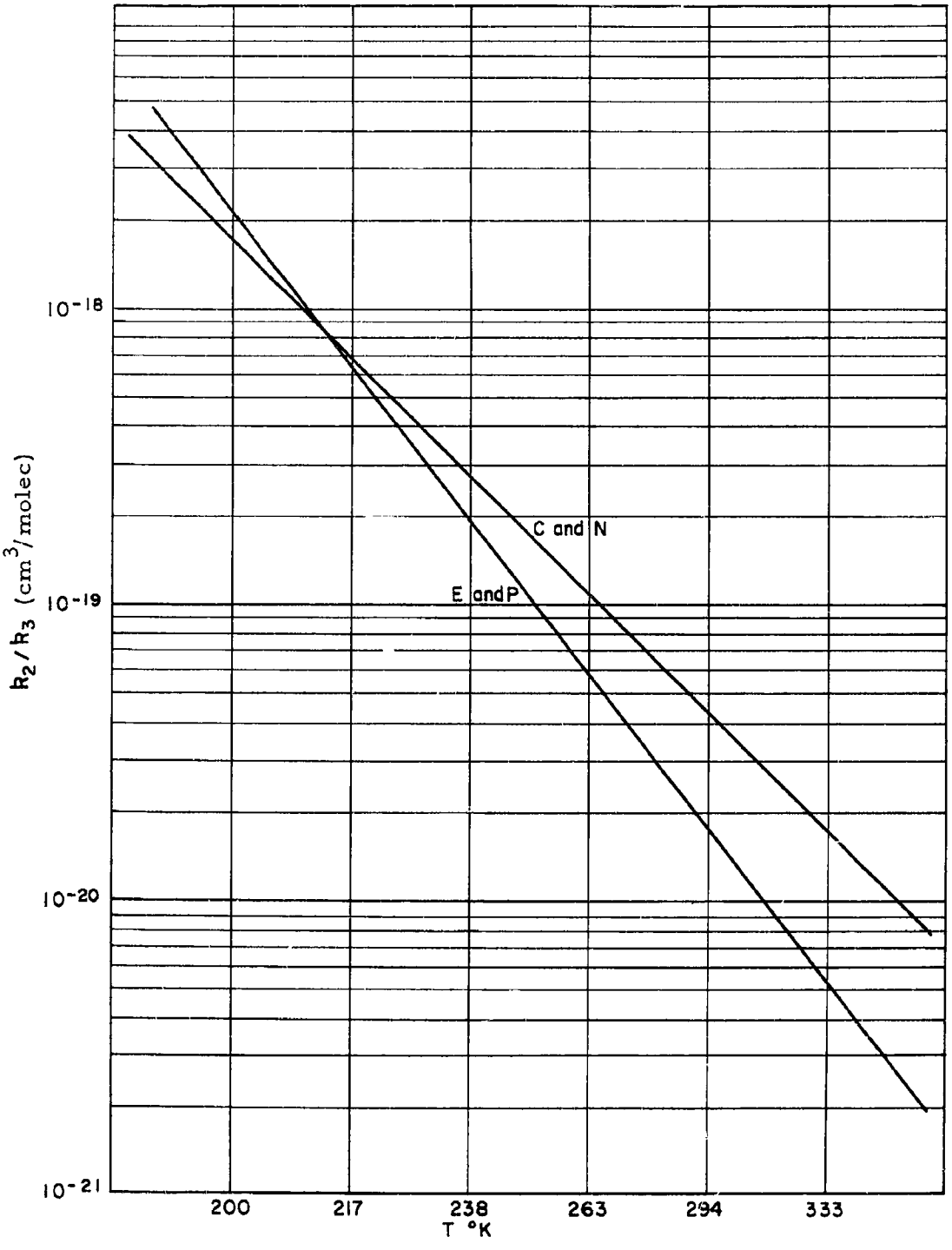

Fig. 2. Variation of the recombination rate ratio k_2/k_3 with temperature after Campbell and Nudelman (C and N) and Eucken and Patat (E and P).

2.4 The model atmosphere

Molecular oxygen was assumed to act as a reservoir for the formation of atomic oxygen and ozone. Consequently, the distribution of molecular oxygen below about 80 km is a function only of the distribution of pressure and temperature. If the concentration of n_2 is taken to be 21 percent of that of total atmospheric particles, we have

$$n_2 = \frac{1}{4.76} \frac{p}{kT}$$
$$= 1.52 \times 10^{18} \, p/T$$

where p is given in mb.

There are sufficient data available to provide for realistic models of the atmosphere up to about 80 km. For the present computations the distribution of pressure and temperature, for winter and summer, was taken from the atmospheric cross sections given by Murgatroyd (1957). These values were extrapolated to polar and equatorial latitudes where necessary.

3. The equilibrium ozone distribution

The photochemical equilibrium distribution of ozone was computed from Eq (11) by a numerical procedure. It was assumed that the ozone concentration above 90 km is zero and that the total depth for molecular oxygen above 90 km is known. Then, since the temperature and pressure is specified at all altitudes and latitudes, the molecular oxygen concentration and the reaction rate coefficients are known for each level. The computation was by iteration starting with the spectral distribution of solar radiation at the top of the atmosphere and computing downward from 90 km in 2-km steps.

The computed distributions depend somewhat on the temperature distribution in the atmosphere and, at some levels, depend rather strongly on the zenith position of the sun. In order to study the effect of this latter relationship, the photochemical distribution was computed for the temperature distribution of 0° latitude for various solar zenith angles. The results are shown in Fig. 3. The curves marked $\zeta = 0°$, 57°, 86.75° correspond to noon at the equator during the equinoxes, mean zenith angle at the equator at summer (winter) solstice, and mean zenith angle at 60° at winter solstice respectively.

It can be seen from the variation of the curves in Fig. 3 that there is marked solar control of the equilibrium distribution below about 45 km. All curves show the well recognized pattern of increasing ozone to a maximum and then a sharp decrease above. The equilibrium maximum results from the dissociation of molecular oxygen in that part of the Herzberg continuum where the ozone absorption is a minimum (2000 - 2200 Å). As a result, solar energy can penetrate downward to about 25 km for a vertical sun and to about 35 km for a highly oblique sun. Also, for large optical paths (high zenith angles) the solar radiation is strongly depleted and the equilibrium ozone value at the level of the maximum concentration is down by a factor of about 30 from the peak at vertical incidence (3×10^{11} cm^{-3} as compared to 10^{13} cm^{-3}).

The general shape of the ozone distribution curves as well as the decrease in ozone concentration and the increase in the height of maximum concentration with increasing zenith angle follow the pattern of a typical "Chapman layer" first derived to describe the formation of layers in the ionosphere (Chapman, 1931).

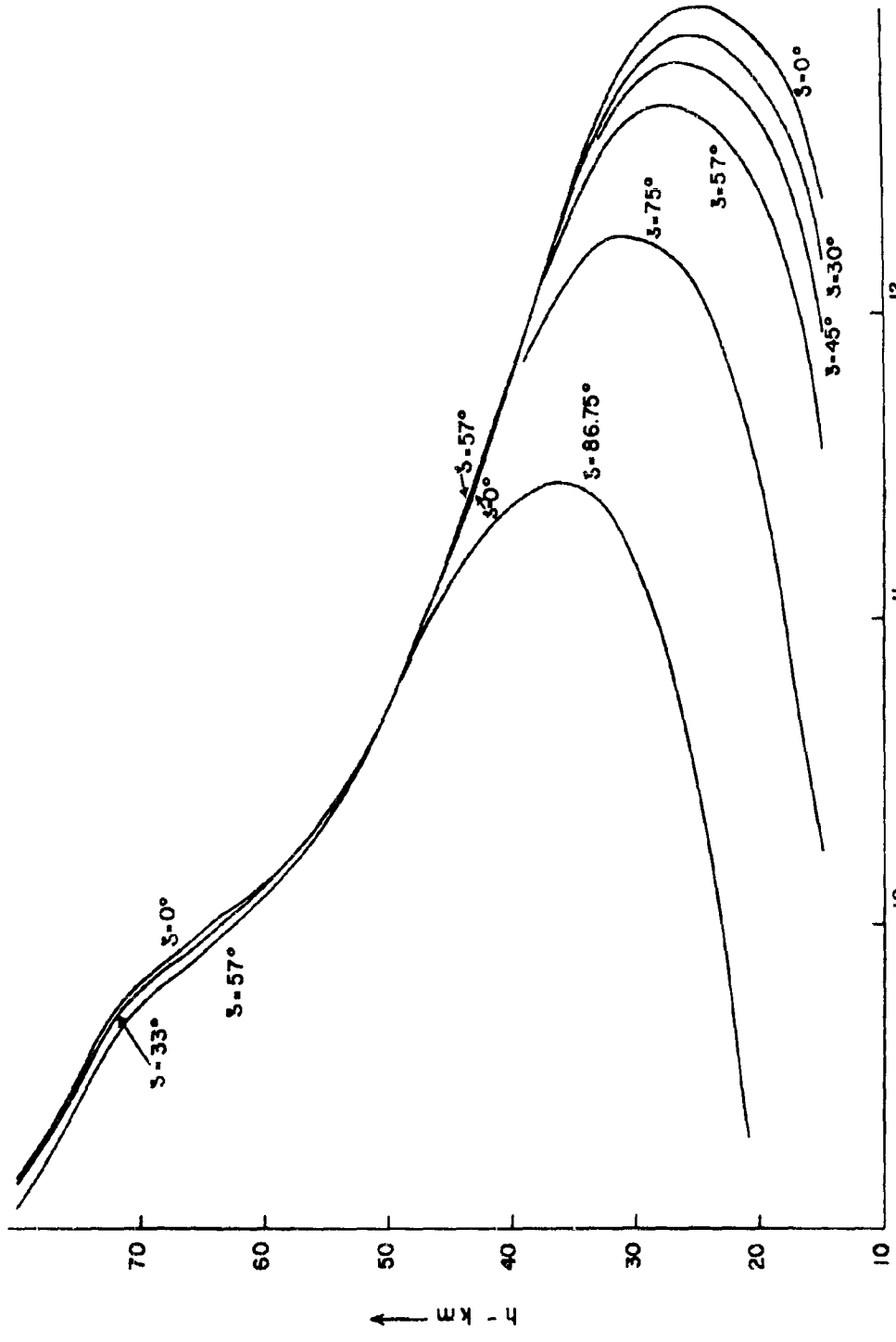

Fig. 3. The photochemical equilibrium distribution of ozone for various solar zenith angles. (The temperature distribution corresponds to that for latitude 0°.)

It can be seen that in the region 45-55 km, the ozone distribution is independent of zenith angle. Above this level, however, increased path lengths through the oxygen atmosphere again result in lower ozone concentrations. The slight bulge in the ozone distribution that appears near 70 km is, in part, due to the strong oxygen dissociation that takes place at the head of the Schumann-Runge band system.

Equilibrium ozone distributions were computed for various latitudes for winter and summer solstices. These are shown in Fig. 4(a) for summer latitudes 0°, 30°, 60°, and 80°; and Fig. 4(b) for winter latitudes 0°, 30°, and 60°. Since the equilibrium concentrations have long half-lives below 45 km, where the solar zenith angles become important, in each computation a mean zenith angle was assumed corresponding to the average angle between sunrise and sunset for the winter (summer) solstice. The average zenith angle used for each latitude is indicated in the legend in Figs. 4(a), (b). The seasonal and latitudinal variations are quite marked, particularly below 40 km and above 60 km. The largest seasonal variations are, of course, at high latitudes. It should be noticed that at 50 km the computed ozone concentration is reasonably constant at approximately 5×10^{11} molec/cm^{-3}.

At 30 km the ozone concentration at 60° latitude decreases by a factor of about 50 from summer to winter (but only by a factor of 10 if the peak concentrations are compared). At 70 km, the decrease in photochemical ozone concentration from summer to winter at high latitudes is about fourfold.

Although the variations in the vertical distributions shown in Fig. 4(a), (b) are mostly due to the effect of solar zenith angle, the atmospheric temperature distribution could, through the temperature sensitive

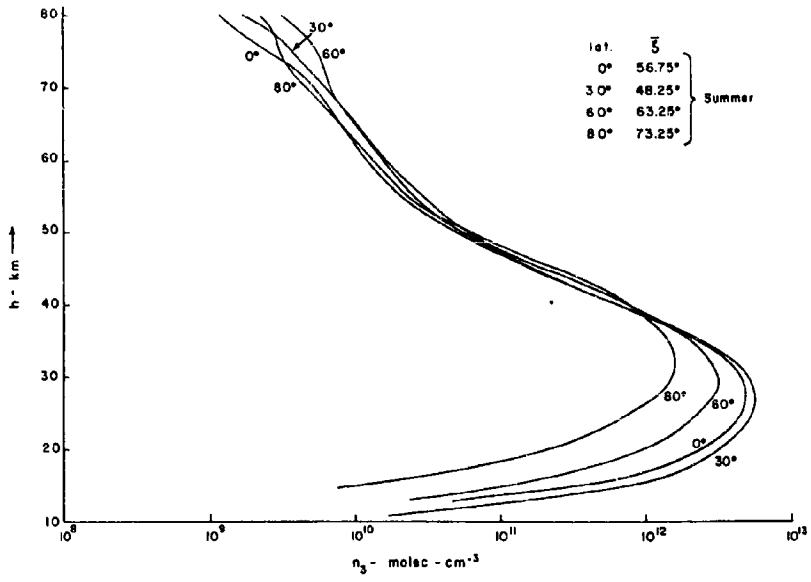

Fig. 4(a) The photochemical equilibrium distribution for ozone corresponding to latitudes 0°, 30°, 60°, 80°. Summer

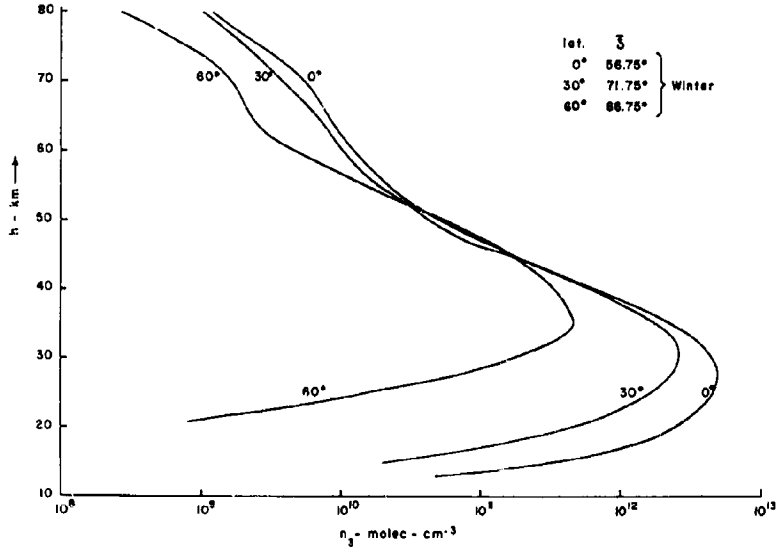

Fig. 4(b) The photochemical equilibrium distribution for ozone corresponding to latitudes 0°, 30°, 60°. Winter

recombination rate coefficients, also affect this distribution. The most important is the rate ratio $k = k_2/k_3$, which decreases over two orders of magnitude for an increase of 100°C in atmospheric temperature.

The temperature effect on the computed vertical ozone distribution is shown in Fig. 5(a). The computations were made for a temperature distribution corresponding to 30° summer and 30°winter. In order to isolate the temperature effect, the average zenith angle $\zeta = 45°$ was used for both computations. The assumed temperature structure is shown in Fig. 5(b). Despite the fact that there is a larger temperature variation below 50 km than above, the effect on the computed ozone distributions is negligible below 50 km and results in about a 20 percent reduction above. This is because at levels below 50 km, the production of ozone is very sensitive to the available solar energy in the region of important overlapping oxygen and ozone absorption (i. e., 2000-2400 Å). Thus, initially higher temperature results in smaller recombination to form ozone which gives less ozone and therefore deeper penetration of the solar beam. This results in more energy being made available to produce slightly more ozone in the level below. There is, therefore, an efficient self-regulating mechanism that produces rather stable equilibrium ozone concentrations despite possible temperature changes at or just below the stratopause (50 km). The consequence of this stable reaction for direct heating of the upper stratosphere has been discussed by Craig and Ohring (1958), who show that this effect will inhibit large temperature changes in the vicinity of the stratopause.

In the region above 60 km, the situation is somewhat different. As before, higher initial temperatures result in lower ozone concentrations. At these heights, however, the dissociation of molecular oxygen

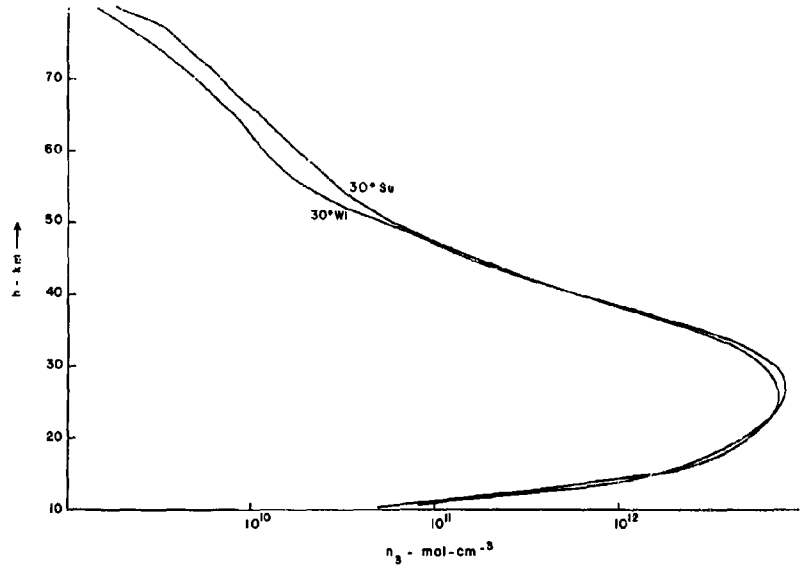

Fig. 5(a) The photochemical equilibrium distribution of ozone corresponding to the temperature structures for 30° winter and 30° summer. (Calculated for $\zeta = 45°$)

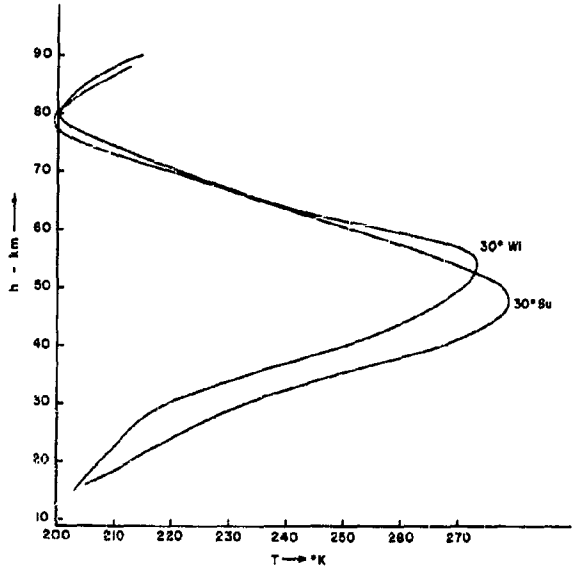

Fig. 5(b) The temperature structures for 30° winter and 30° summer for the curves of 5(a).

is produced by absorption at wavelengths where the depletion of solar radiation by the total ozone column is not very important (i.e. $\lambda < 1900$ Å). Lower ozone concentrations above 60 km, therefore, have relatively little effect on the available energy at these levels. Thus, the influence of higher temperatures such as found at high latitudes in the mesosphere during winter as compared to summer, particularly when combined with the effect of increased zenith angles, result in decreased equilibrium ozone amounts in the upper mesosphere. (Compare, for instance, Figs. 4(a) and 4(b).) In the absence of any self-regulating mechanism, some anomalous heating of the air in the mesosphere could then result in a decrease of the total ozone above, say, 60 km allowing for a greater penetration of near ultraviolet radiation to the region of the stratopause.

The vertical ozone distributions shown in Figs. 4(a), (b) are very similar to those given by Dütsch (1956), with two notable exceptions. The level of maximum ozone is, in all cases, higher in the present calculations, and at the level of maximum ozone concentration and above, the present calculations give larger ozone amounts than those computed by Dütsch. Below the maximum level, Dütsch's values are larger. Both of these differences stem primarily from the differences in model atmospheres (temperature distribution) assumed and the present absorption cross sections used for the computations.

4. The absorption of solar radiation by atmospheric oxygen and ozone

Monochromatic solar radiation in the spectral region (1700 - 3000 Å) is depleted as it penetrates through the mesosphere chiefly by absorption by molecular oxygen and ozone. In that case, the transmission

of solar radiation down to any atmospheric level is, from Eq (8a, b), as

$$\tau_\lambda(Z) = q_\lambda(Z)/q_\lambda(\infty) = \exp\left[-(\sigma_{\lambda 2} N_2(Z) + \sigma_{\lambda 3} N_3(Z)\right] \qquad (14)$$

The depth of penetration of solar radiation in the atmosphere was computed for the spectral region 1720 Å to 3100 Å for an atmospheric transmission of 5 percent (i. e., assuming that 95 percent of the solar energy is absorbed in the layer above the level indicated) and for various latitudes and seasons. N_3 was calculated from the equilibrium distributions as discussed above. The results are shown in Fig. 6 for two of the extreme cases, those of 30° summer and 60° winter. The portion of the curves lying above 85 km is quite unreliable since it depends strongly on the total number of oxygen molecules above this level. This is the region where oxygen dissociation is quite strong, and there is probably large variation in the molecular oxygen concentration due to vertical motions and associated recombination processes.

The difference in the depth of penetration shown by the two curves is roughly constant at about 10 km. This means that, on the average, the seasonal and latitudinal variations of the penetration of solar radiation can be as large as about 10 km. The difference in penetration through the strong Schumann-Runge bands due to molecular oxygen absorption is quite evident. It is seen that some solar energy can filter down through the absorption minima to levels of about 60 km.

The most important region as far as ozone production is concerned is the region of absorption overlap (2000 - 2200 Å) where the Herzberg continuum absorption has become quite weak, and the ozone absorption cross section at the short wave portion of the Hartley band has its minimum value. In this spectral region, only 5 percent of the solar energy

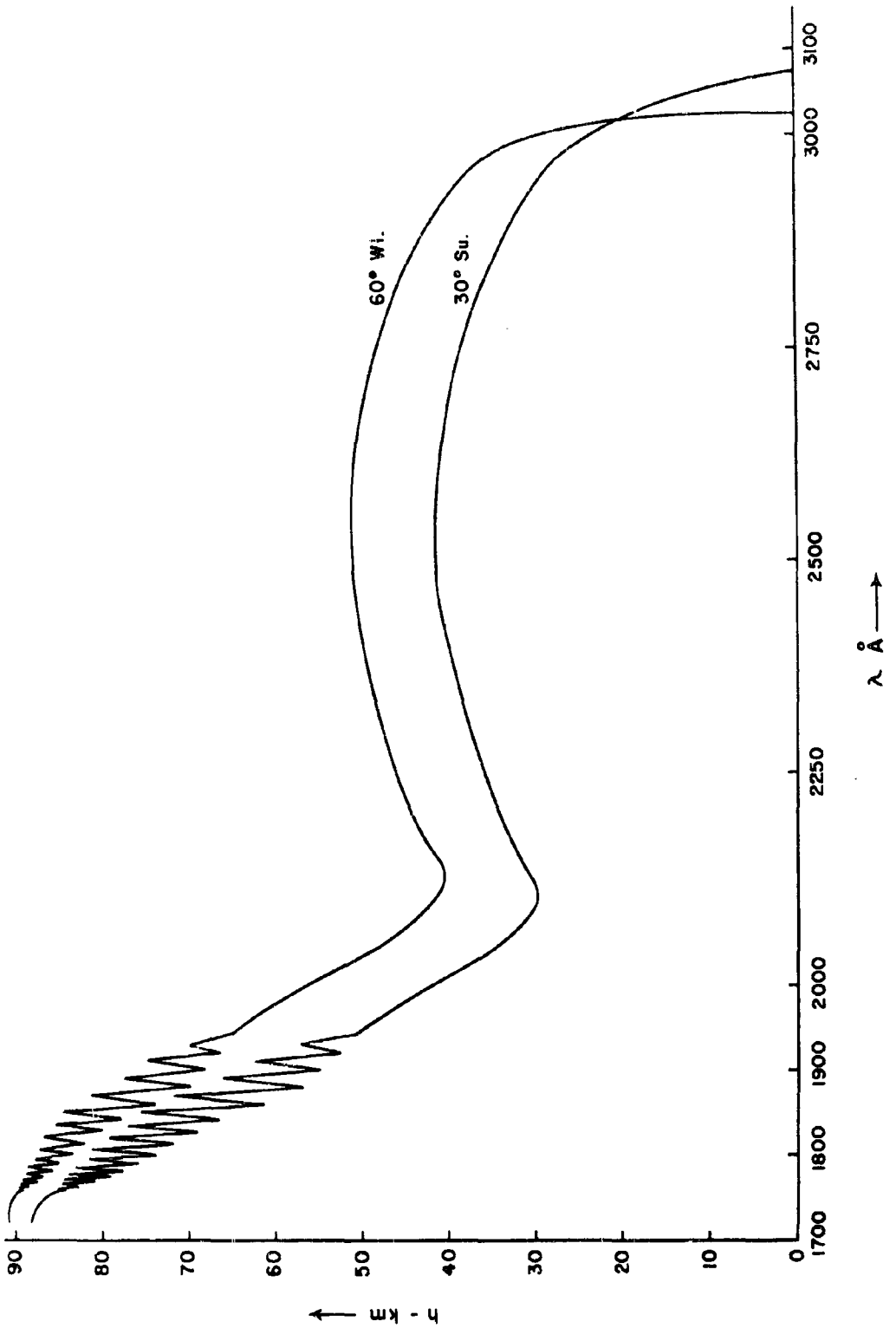

Fig. 6. The spectral distribution of depth of penetration for solar radiation assuming atmospheric transmissivity of 5 percent. The two curves are for mean conditions corresponding to 30° summer and 60° winter.

received at the top of the atmosphere penetrates to levels much below 35 km. At the time of high sun, the solar radiation is able to penetrate somewhat deeper into the stratosphere. Although 3-body recombination at these heights is rather rapid, there is insufficient energy for large-scale dissociation of molecular oxygen. The result is that the maximum equilibrium amount of ozone is found at levels just under 35 km. Below the level of maximum ozone there is little production of atomic oxygen and the ozone concentration falls rapidly.

The influence of the strong Hartley absorption bands can be seen in the shape of the penetration curve in the region 2200-3000 Å. Very little solar energy of wavelength 2550 Å can penetrate below about 40 km. The strong absorption even at the top of the stratosphere (about 50 km) results in the relatively high temperatures found at the stratopause. Again, the relative height difference of constant atmospheric transmissivity in this spectral interval is approximately what one finds for the height difference of the level of maximum temperature between equatorial regions and high latitude winter. Since we have seen that the ozone concentration is not sensitive to the temperature at these levels, the temperature structure in the region of the stratopause must result from the ozone distribution and the absorption of solar energy at these heights and latitudes.

The two curves in Fig. 6 cross at about 3000 Å. This results from the fact that the photochemical distribution rather than the actual ozone distribution was used for levels below 25 km. The large slope of the two curves near 3000 Å, however, indicate the important absorption transition region from the Hartley to the Huggins bands.

5. Heating of the upper atmosphere

The processes involved in the reactions described in Eqs (1-5) are such that the energy exchanged in photochemical dissociation and recombinations are always almost in balance so that the solar energy absorbed during the day is almost completely used to increase the kinetic energy of the absorbing molecules. This results in a temperature change of the air at the levels where the energy is absorbed.

The total absorption per unit volume at any level by molecular oxygen and ozone is then given by

$$E_2(Z) = \int_\lambda N_2 \sigma_{2\lambda} E_\lambda^{(\infty)} \exp\left[-\sigma_{2\lambda} N_2 - \sigma_{3\lambda} N_3\right] d\lambda \qquad (15a)$$

$$E_3(Z) = \int_\lambda N_3 \sigma_{3\lambda} E_\lambda^{(\infty)} \exp\left[-\sigma_{2\lambda} N_2 - \sigma_{3\lambda} N_3\right] d\lambda \qquad (15b)$$

where $E_\lambda^{(\infty)}$ represents the available solar energy at the top of the atmosphere in ergs $cm^{-2} sec^{-1} \mathring{A}^{-1}$, and the integration is taken over all wavelengths for which the factors $\sigma_{2\lambda} E_\lambda^{(\infty)}$ and $\sigma_{3\lambda} E_\lambda^{(\infty)}$ are significantly different from zero (i.e., $1700\,\mathring{A} \leq \lambda \leq 2424\,\mathring{A}$ for E_2, and $2000\,\mathring{A} \leq \lambda \leq 7500\,\mathring{A}$ for E_3).

The heating of the atmosphere at any level is given by the absorption per unit mass. Thus, the total heating during the day is

$$H(Z) = 2 \int_0^{\omega_o} \frac{g}{C_p} \frac{E(Z)}{\Delta p} \, d\omega \qquad (16)$$

where ω is the hour angle of the sun (ω_o represents the local hour angle at sunrise or sunset) and Δp is the pressure difference between the top and bottom of the layer in which the absorption occurs. For the computations it was assumed that the molecular oxygen concentration

is constant during the day, that the local ozone concentration is also constant during the day and is given by the photochemical equilibrium distribution at all levels. This latter assumption is probably reasonably correct down to about 40 km below which the distribution begins to depart radically from photochemical equilibrium.

Heating computations were made separately for molecular exygen and ozone. It was found that atomspheric heating due to solar energy absorption by molecular oxygen is completely negligible in the stratosphere and mesosphere when compared to heating due to absorption by ozone. For example, the heating rate due to oxygen absorption is at most 1-2 degrees per day during the summer at about 80 km and decreases rapidly with decreasing height. On the other hand, heating due to ozone absorption is of the order of 10-20 degrees per day through most of the stratosphere and mesosphere (except for high latitudes during the winter). At levels above 80 km, however, the oxygen absorption becomes important and as the ozone concentration goes to zero, the heating of the lower layers of the thermosphere is due primarily to absorption by molecular oxygen in the spectra intervals $\lambda < 1800$ Å.

The distribution with height and latitude of the calculated heating rates are shown as a summer-winter cross section in Fig. 7. The values are given in °C/day for combined absorption due to molecular oxygen and ozone.

It can be seen from Fig. 7 that the rate of heating is a maximum at the stratopause and is about 16°C/day at high latitudes during the summer decreasing to about 3°C/day at 60° during the winter. The level of maximum heating is lowest at the equator (about 45 km) and highest (about 55 km) at high latitudes during the winter. Above this

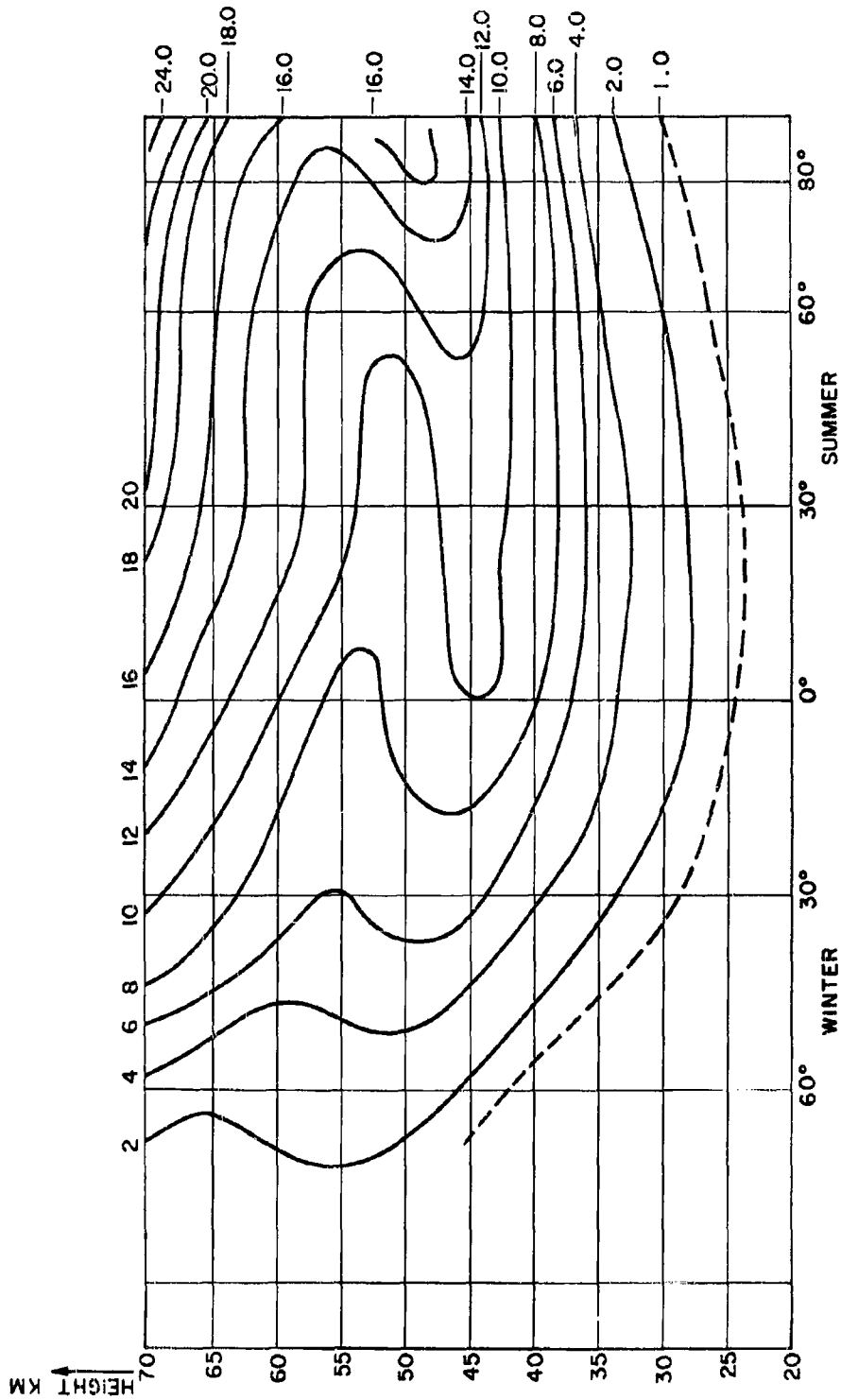

Fig. 7. The distribution of heating due to absorption of solar radiation by O_3 and O_2 (°C/day).

region of maximum heating there seems to be a shallow layer of decreased heating rate and then a deep layer of strong heating, particularly at high latitudes during the summer. Below 45 km the heating values are everywhere decreased being less than 2°C/day below 27 km.

It should be pointed out that the computed heating rates are somewhat unreliable at levels below about 35 km because of the strong departures from photochemical equilibrium concentrations.

At levels above 60 km, the indicated temperature changes due to absorption of solar radiation could be incorrect by as much as an order of magnitude. At these elevations the ozone distribution again departs somewhat from photochemical equilibrium, and as was pointed out above, the value used for the recombination rate ratio, k_1/k_2, was probably much too small. In addition, secondary reactions involving H, OH, and NO have been neglected in the photochemical computations (see, for instance, Horiuchi, 1961; Wallace, 1962). These effects would all tend to reduce the amount of ozone present and reduce the heating in the mesosphere, particularly above 65 km. The computed heating rates in the region of 35-60 km, however, are quite realistic and are quite clearly reflected in the temperature pattern at these levels.

References

Campbell, E. S., and C. Nudelman, 1960: Reaction kinetics, thermodynamics, and transport properties in the ozone-oxygen system. AFOSR TN-60-502, Department of Chemistry, New York University, N. Y.

Chapman, S., 1930: A theory of upper atmospheric ozone. Mem. Roy. Met. Soc., 3, 103-125.

Chapman, S., 1931: The absorption and dissociative or ionizing effect of monochromatic radiation in an atmosphere on a rotating earth. Proc. Phys. Soc. (London), 43, 26-45.

Craig, R. A., 1950: The observations and photochemistry of atmospheric ozone and their meteorological significance. Met. Monog., 1, No. 2, 50, Am. Met. Soc.

Craig, R. A., and G. Ohring, 1958: The temperature dependence of ozone radiational heating rates in the vicinity of the mesopeak. J. Meteor., 15, 59-62.

Detwiler, D. R., D. L. Garrett, J. P. Purcell, and R. Tousey, 1961: The intensity distribution in the ultraviolet solar spectrum. Annales de Géophysique, 17, 263-272.

Dütsch, H. U., 1956: Das atmosphärische Ozon als Indikator für Stromungen in der Stratosphäre. Archiv für Met., Geophys. u. Bioklimat., A, 9, 87-119.

Eucken, A., and F. Patat, 1936: Die Temperaturabhangigkeit der photochemischen Ozonbildung. Z. f. Phys. Chemie., 33, 459-474.

Götz, F. W. P., 1951: Ozone in the atmosphere. Compendium of Meteorology, ed. by T. F. Malone, Am. Met. Soc., 275-291.

Horiuchi, G., 1961: Odd oxygen in the mesosphere and some meteorological considerations. Geophys. Mag., 30, 439-520, Japanese Meteor. Agency, Tokyo.

Inn, E. C. Y., and Y. Tanaka, 1953: Absorption coefficients of ozone in the ultraviolet and visible regions. J. Opt. Soc., 43, 870-873.

Johnson, F. S., 1954: The solar constant. J. Meteor., 11, 431-439.

Johnson, F. S., J. D. Purcell, R. Tousey, and N. Wilson, 1954: The ultraviolet spectrum of the sun. Rocket Exploration of the Upper Atmosphere, 274-288, ed. by Boyd, R. L. F. and M. J. Seaton, Pergamon Press, London.

Murgatroyd, R. J., 1957: Winds and temperatures between 20 km and 100 km. Q. J. Roy. Met. Soc., 83, 417-458.

Vigroux, E., 1953: Contribution a l'étude expérimentale de l'absorption de l'ozone. Annales de Physique, 8, 709-762.

Wallace, L., 1962: The OH nightglow emission. J. Atmos. Sci., 19, 1-16.

Watanabe, K., 195k: Ultraviolet absorption processes in the upper atmosphere. Advances in Geophys., 5, 153-221.

Wulf, O. R., and L. S. Deming, 1936: The theoretical calculation of the distributions of photochemically-formed ozone in the atmosphere. Terr. Mag., 41, 299-310.

PART III

The Distribution of Total Ozone in the Northern Hemisphere

by

J. London

1. Introduction

Measurements of total ozone in a vertical column in the atmosphere have been made since about 1921 (Fowle, 1928). The first set of consistent observations, however, resulted from a standardized program developed in 1924 by Professor G. M. B. Dobson at Oxford, England (Dobson and Harrison, 1926). This observational program was based on a spectrographic technique which made use of a method first suggested by Fabry and Buisson (1921) whereby the total ozone was calculated from observations of solar radiation (or radiation from any stellar source) in the region of the Huggins ozone absorption bands (≈ 3200 Å). Dobson made use of the fact that if the received light intensity is measured at two different wavelengths (one of strong, the other of weak absorption), the calculated total ozone is proportional to the logarithm of the intensity ratio and inversely proportional to the difference in absorption coefficients at the two different wavelengths.

In 1926 the ozone observing program was extended to a few selected places in both hemispheres, and for the next twenty-five years routine observations were taken at only a few stations. An organized observational program involving a network of ozone observing stations (mostly in Europe) was started by the then International Meteorological Organization, in 1951. At the start of the IGY program (1957) there were about twenty stations throughout the world taking regular daily total ozone observations. Since then this number has more than

doubled. There are now approximately 50 stations observing and reporting total ozone values on a routine basis, and the number is constantly increasing.

The fundamental observing method developed by Dobson is still used today by the extensive ozone observing network, although a number of basic improvements in the instrumentation were made with the introduction in 1931 of the spectrophotometer and the new photo-electric instrument in 1939. The presently used instrument and a description of the technique of its use is given by Dobson (1957).

Soon after the first observations it was discovered (Dobson, et al. 1926; Fowle, 1928, 1929) that the vertically integrated total ozone amount had large day-to-day variations but on the average was a maximum during the spring and a minimum during the fall. As a result of the carefully planned observational program, Dobson and his colleagues (Dobson, et al. 1928) were also able to show that this seasonal variation prevailed in the Southern Hemisphere and that total ozone values were, on the average, greatest at sub-polar latitudes ($\approx 60°$) and least near the equator. Their studies clearly indicated that total ozone is related to synoptic pressure patterns at the surface and aloft. High ozone amounts tend to occur with low surface pressure; low ozone amounts tend to occur with high surface pressure. Later studies have substantiated these relationships for various regions and conditions. Moreover, it has been shown that the correlations between ozone and pressure and temperature patterns aloft are invariably larger during winter and spring than during summer and fall seasons.

Although the strong latitudinal gradient of ozone was noticed early in ozone research, it was first suggested by Haurwitz (1938)

in comparing ozone observations taken at Shanghai with those taken in Western Europe that there might be a longitude variation in total ozone as related to surface pressure patterns. This possible longitude variation was again noted by Craig (1950) and has since been verified by many for specific regions. (See, for instance, Kulkarni, et al, 1959.)

2. Ozone data

The increased number of ozone observations in recent years has made it possible to study the distribution of total ozone over the entire Northern Hemisphere. In order to get as widespread coverage of the data as possible it is necessary to use all of the available ozone observations that could be put into a consistent set.

It was mentioned earlier that the calculated ozone amount is inversely proportional to the adopted valuc of the difference in ozone absorption coefficients for the two wavelengths at which measurements are taken. That is, X cm of ozone is proportional to $1/(\alpha - \alpha')$.

The early observations directed by Dobson made use of absorption coefficients reported by Fabry and Buisson (Dobson et al, 1926). Later, results of Ny and Choong (1932) were used which gave slightly lower computed ozone amounts. More recently, careful laboratory measurements by Vigroux (1953) and Inn and Tanaka (1953) have given absorption values substantially lower than those reported by Ny and Choong. The absorption coefficients of Vigroux have been adopted by the World Meteorological Organization for all measurements

made after 1 July 1957. Consequently all observations prior to that time have been corrected to be consistent with the Vigroux coefficients.

Total ozone values are reported here in Dobson units (10^{-3}cm NTP). This is the equivalent depth of a layer of ozone if all the ozone molecules in a unit vertical column were brought to normal temperature and pressure (0°C, 1013 mb).

Although there are a few partial sources for total ozone data, (see for instance, Craig, 1950) most of the data are scattered throughout the literature, much of it still unpublished. An attempt was therefore made to collect and tabulate all of the available data together with the sources of information. In this endeavor we were helped greatly by the kind cooperation of Sir Charles Normand and Professor G. M. B. Dobson then secretary and president repsecti vely of the International Ozone Commission. The sources and data are tabulated as appendix A and B at the end of this report. The source list is given only for data prior to the start of the IGY (1 July 1957) since almost all data taken subsequent to this date (July 1957 - December 1959) have been tabulated by the World Meteorological Organization. Arrangements are currently being made by WMO to have the data published as annual summaries. All pre-IGY data, which were formally tabulated according to the Ny-Choong absorption values, have been multiplied by the factor 1.35 to make the data consistent with the new Vigroux scale (see Perl and Dütsch, 1959).

5. The hemispheric ozone distribution

The data for the distribution of total ozone over the Northern Hemisphere have been analyzed for the whole year and for each of the

four seasons. The data used were the totality of observations made at the various stations from the start of their observations through 1959, corrected when necessary to be consistent with the new (Vigroux) absorption coefficients presently being used with the Dobson spectrophotometer as discussed above. The analysis is given in Figs. 1(a) - (d) for winter (Dec, Jan, Feb); spring (Mar, Apr, May); summer (Jun, Jul, Aug.); fall (Sep, Oct, Nov); and in Fig. 2 for a composite annual distribution.

Total ozone is seen to be a minimum at the equator (about 240 DU) and generally to increase poleward during all seasons. In general, the latitudinal gradient is a maximum during the spring and minimum during the fall. In polar regions there are three centers of high ozone amounts found at about 60°N over Eastern Canada, North Central Europe and Eastern Siberia. The strength of these centers increases from winter to spring (to a maximum of about 460 DU) and then decreases from spring to fall. Near the equator, and during all seasons, there is relatively little longitude variation in total ozone. For instance, Marcus Island (24°N 154°E) and Mauna Loa (19°N 155°W) have practically identical ozone amounts during all seasons of the year. At higher latitudes, however, this is not so. There seems to be at least three well developed ozone ridges extending from the high ozone centers mentioned above. These ridges are found in the vicinity of the east coasts of North America and Asia and in Central Europe. Although the ridges are semipermanent features of the ozone distribution, they are best developed during winter and spring [Figs. 1(a), (b)] and least well developed during summer and fall [Figs. 1(c), (d)].

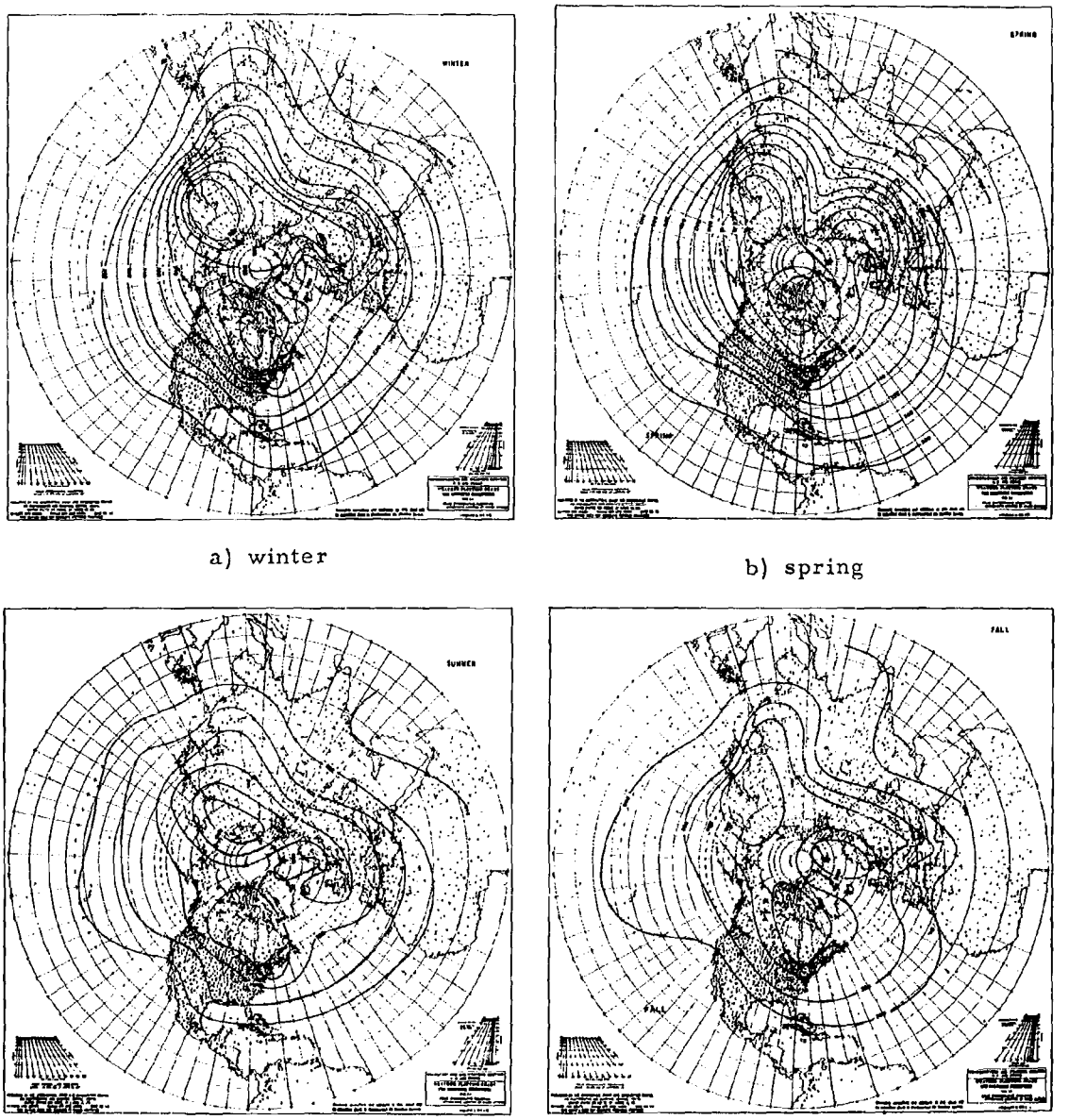

a) winter

b) spring

c) summer

d) fall

Fig. 1. The distribution of total ozone in the Northern Hemisphere (1926-1959). Dobson units (10^{-3} cm NTP).

Comparison between the maps showing hemispheric distribution of ozone and maps of the general circulation of the upper troposphere and lower stratosphere (Wahl 1958, Panofsky 1960) shows that particularly during the winter and spring, there are three well developed contour troughs at all levels from 200 mb to 50 mb located in the same general regions as for the ozone ridges. During the summer and fall, however, although the contour troughs appear at 200 mb, they have completely disappeared in the upper level maps. There is, thus, indication for a reasonably strong coupling mechanism between the development of the semipermanent trough pattern at upper levels and the total ozone pattern discussed above. The dashed lines shown in Fig. 2 are extrapolations to regions where there are no data. It is hoped that as more data become available the area of uncertain analysis will become less and less.

The low ozone anomaly that appears over the Scandinavian peninsula does not seem to have any well defined relation to the upper air circulation pattern. It may be that there is a strong local bias in the observations such that intervals of low pressure are accompanied by persistent low cloudiness and rain which would prevent accurate ozone observations. Because of the inverse relationship between pressure and ozone, this sampling bias would result in unrepresentative low ozone values. This is particularly true for the earlier observations when the various cloud corrections were not clearly defined. More recent data (as discussed below for the period 1958-59) show a slight ozone trough in the general vicinity of the Scandinavian peninsula but not nearly as pronounced as those shown in Figs. 1(a) -(d).

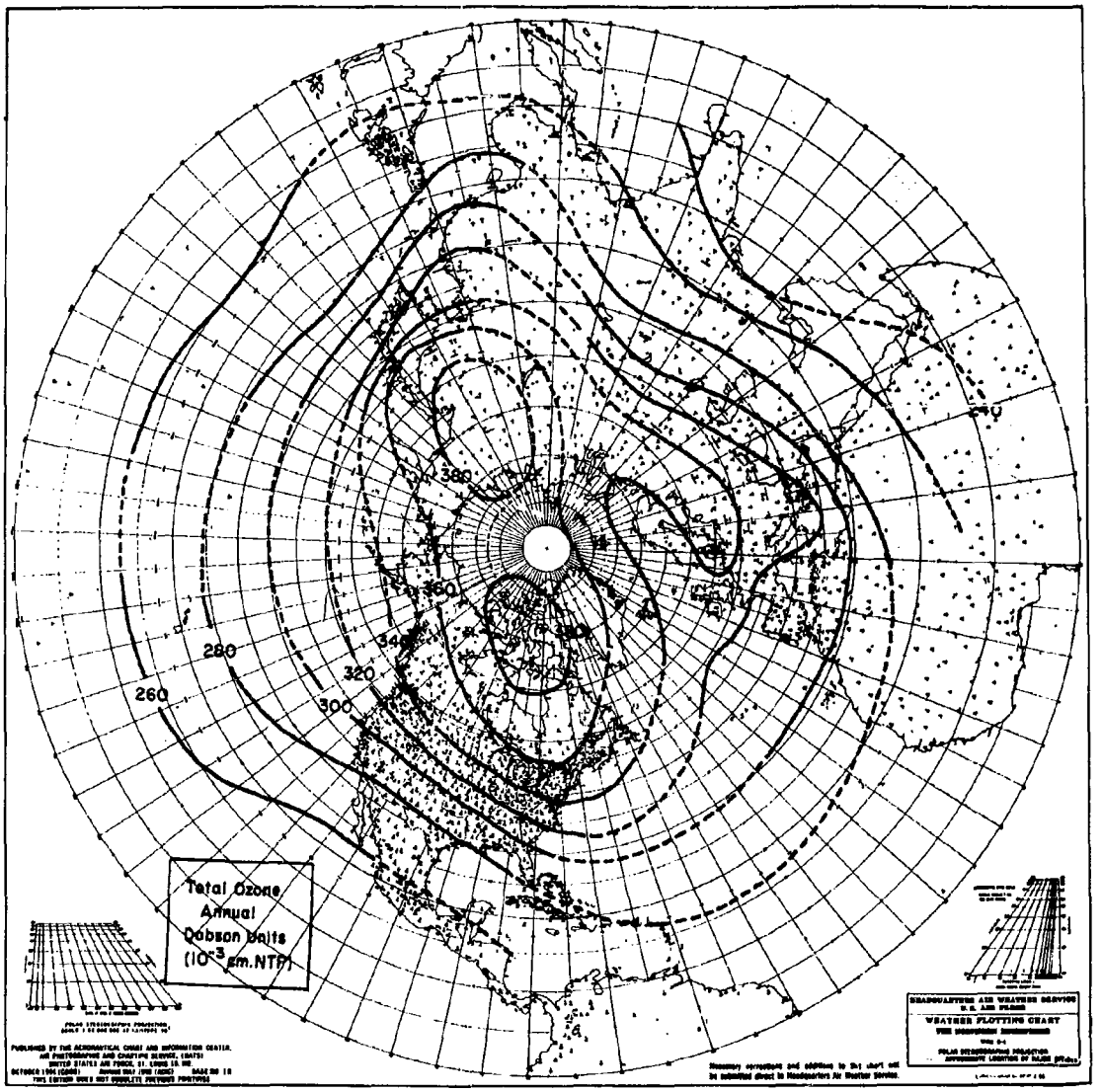

Fig. 2. The same as Fig. 1 --- annual.

As was pointed out above, in an attempt to get widespread coverage for analysis of the ozone maps, all available data up to 1959 were used. In this grouping of data there were many stations that had only one or two years of observations and only one station (Arosa, Switzerland) that had over 30 years of data. This inhomogeneous set raises the problem of the representativeness of the data. The two longest records of data are those for Arosa (32 years) and Tromso (24 years). When the monthly values are grouped according to season, the number of years for which there are data is decreased. The least number of years for which data are available is, of course, for the annual means. The following table gives a measure of the inter-annual seasonal and annual variation of ozone amounts for three stations of longest record.

Table 1. Standard deviation of seasonal and annual total ozone values (DU).

Station	Winter		Spring		Summer		Fall		Annual	
	σ	N	σ	N	σ	N	σ	N	σ	N
Tromso, Norway (70°N)	51	12	20	21	15	20	15	16	18	10
Oxford, England (52°N)	12	9	17	13	10	12	12	10	8	9
Arosa, Switzerland (47°N)	14	29	14	30	8	29	7	30	9	27

It should be pointed out that in most cases the number of years available to compute the standard deviation was quite small and the values given in Table 1 are reliable, if at all, only in a qualitative sense. Three general characteristics of the ozone data, however, are suggested by the numbers in Table 1. The variation of the data:

a) increases with increasing latitude
b) is larger during winter and spring than summer and fall
c) is about 20 DU .

The first two characteristics mentioned above are in general agreement with our knowledge of total ozone variations. The size of the standard deviation indicates the representativeness of the analysis shown in Figs. 1(a)-(d) and Fig. 2. Since the presence of the high ozone centers and the approximate placement of the ozone ridges result from ozone differences much larger than 20 DU there is no question about the reality of the general topography of the longitude variations. However, minor variations in the ozone distribution probably have little basis in fact.

In order to test further the representativeness of the distributions discussed above, a separate set of maps was analyzed for the period 1958-59. These are shown in Figs. 3(a) and 3(b) for the spring and fall. Again dashed lines indicate areas for which there were no data. Although the data available for analysis of Figs. 3(a), (b) were considerably less than for Figs. 1, 2 the advantages are that the data were coherent in time and were taken with improved instruments and presumably more accurate techniques.

The results shown in Figs. 3(a), (b) are substantially the same as discussed above. Again there is a pronounced three wave pattern in the ozone distribution in approximately the same positions as shown before. Also, the spring patterns are much stronger than those for fall. There are some slight differences in central ozone values and the exact positions of the ozone ridges. Although it is probable that there are significant year to year variations in the topography of the ozone distribution, the present set of observations do not permit of such a fine analysis as would determine such variations. The differences between Figs. 1(b), (d) and Figs. 3(a), (b) are certainly much smaller than their similarities.

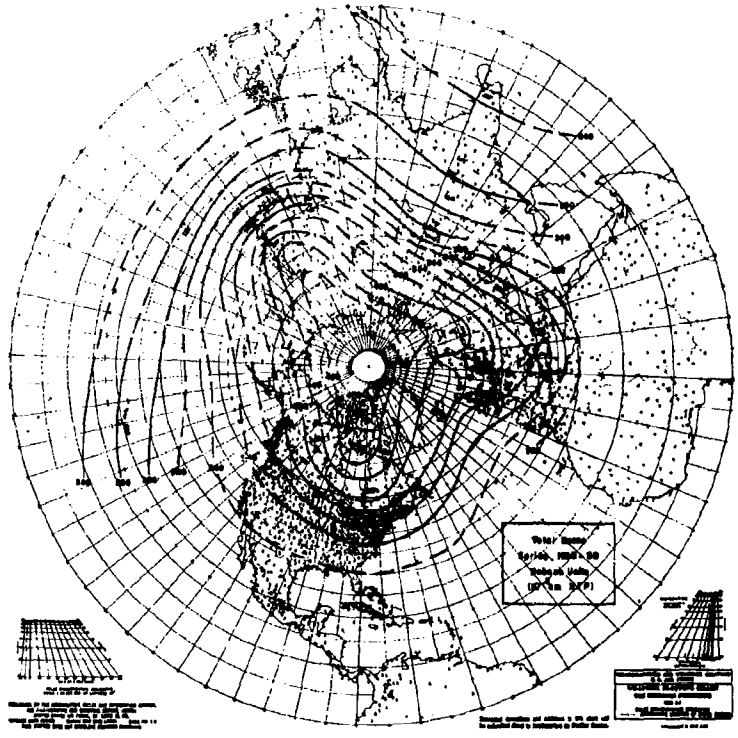

a) spring

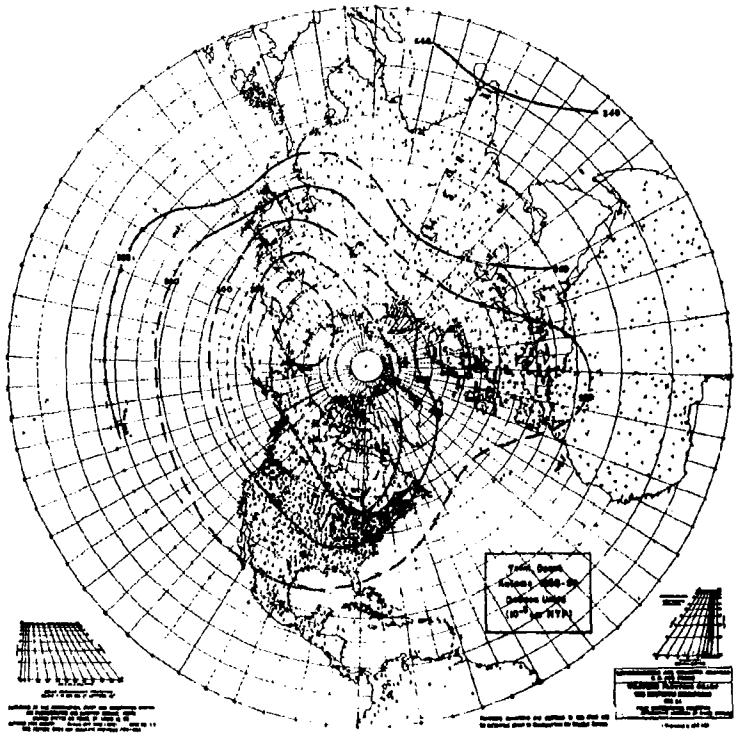

b) fall

Fig. 3. The distribution of total ozone in the Northern Hemisphere (1958-59).

The average total ozone amount around each latitude circle was computed from Figs. 1(a)-(d) and Fig. 2. The results are shown in Fig. 4, giving mean total ozone as a function of latitude for each season and for the annual distribution. The data did not extend much beyond 20° latitude and the lower parts of the curves represent extrapolated values. Also, the fact that the annual curve does not represent the average of the other four curves in the region north of 75° indicates the slight lack of consistency of the analysis in this region. In general, however, the patterns hold together quite well.

During all seasons there is increasing ozone to the north with the maximum indicated at about 60°-70°. The largest gradient is found in middle latitudes (30°-50°) during all seasons but predominantly during spring. Also, it is most noticeable that the seasonal variation is smallest in equatorial latitudes and largest in polar latitudes. If the ozone amounts are averaged over the hemisphere for each of the seasons we find that the observed distribution gives:

Winter	-	298 DU
Spring	-	330 DU
Summer	-	297 DU
Fall	-	274 DU
Annual	-	299 DU

This can be compared to the amount of ozone which would be maintained in a photochemical equilibrium atmosphere. If we integrate the vertical distribution of equilibrium ozone as given in the preceding section for each latitude and the two seasons we get

Summer	-	347 DU
Winter	-	171 DU
Annual	-	259 DU

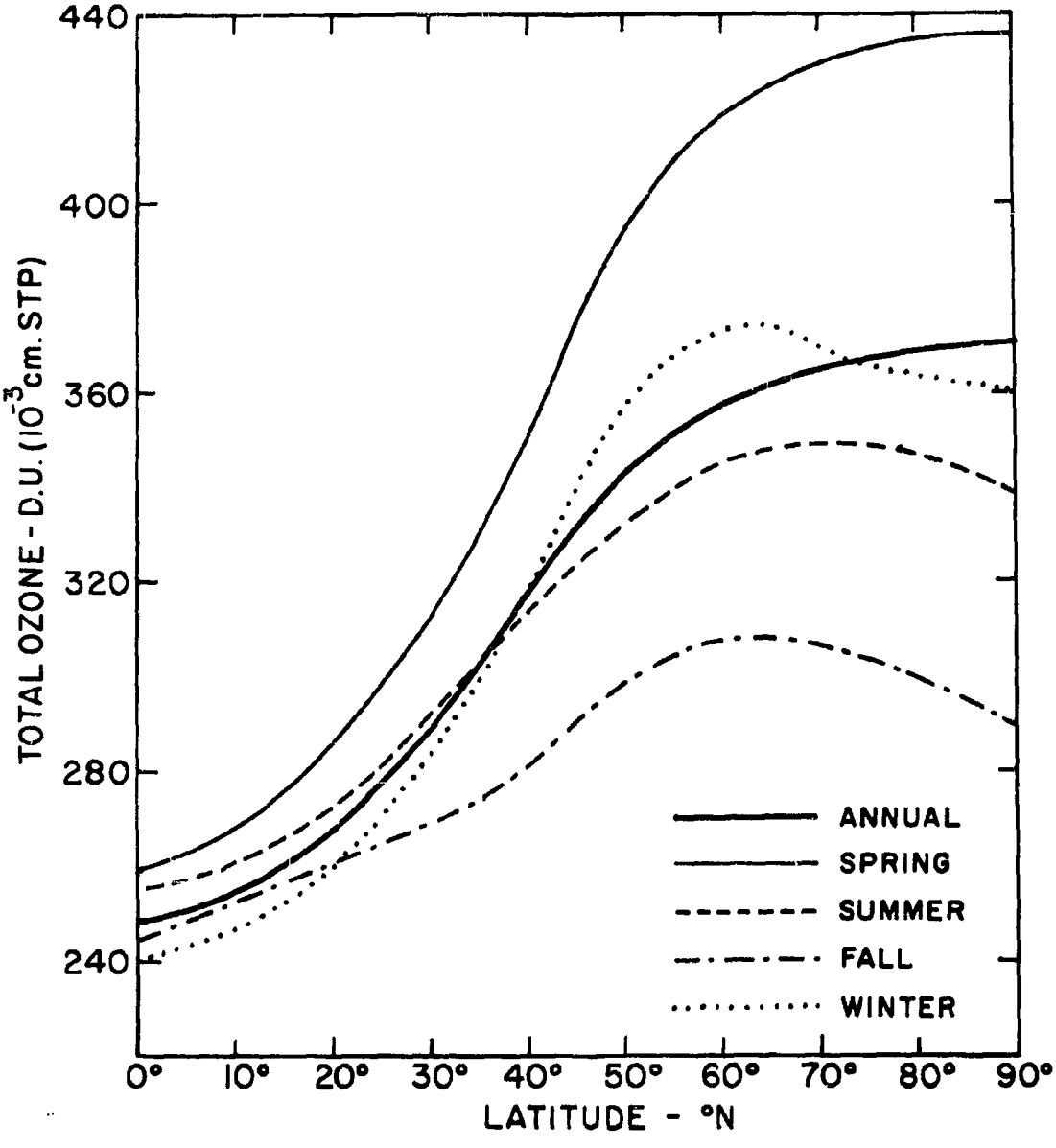

Fig. 4. The average variation of total ozone with latitude.

Although the annual amount is only slightly less than the observed annual amount, of most concern is the marked differences in seasonal and latitudinal variations. Thus, the observable amounts of ozone can be produced by photochemical processes but the temporal and latitudinal distributions most certainly are controlled by the large scale general circulation of the upper troposphere and lower stratosphere. The large scale distribution of total ozone shows a marked relation to the large scale atmospheric pressure systems. Also ozone must be transported from the region of production (equatorial latitudes) to polar regions to account for the observed ozone distribution. Both of these facts indicate that it is most likely that the atmospheric transporting mechanism for ozone is essentially the same as that responsible for maintaining the heat and momentum budgets of the atmosphere. It is of considerable general interest therefore, to probe deeper, as more data become available, into the problem of the relation of the general circulation of the atmosphere and the variations in the ozone budget.

References

Craig, R. A., 1950: The observations and photochemistry of atmospheric ozone and their meteorological significance. Met. Monog., 1, no. 2, 50, Amer. Met. Soc.

Dobson, G. M. B., and D. N. Harrison, 1926: Measurements of the amount of ozone in the earth's atmosphere and its relation to other geophysical conditions. Proc. Roy. Soc., 110, 660-693.

Dobson, G. M. B., D. N. Harrison, and J. Lawrence, 1928: Measurements of the amount of ozone in the earth's atmosphere and its relation to the geophysical conditions. Proc. Roy. Soc., A, 122, 456-486.

Dobson, G. M. B., 1957: Observator's handbook for the ozone spectrophotometer. Ann. of the IGY, V, part 1, sec. 3, 46-89.

Fabry, C., and M. Buisson, 1921: Étude de l'extrèmité ultraviolet du spectre solaire. J. Phys. Rad., Ser. 6, 2, 197-226.

Fowle, F. E., 1928: Ozone in the Northern and Southern Hemispheres. Journ. of Terr. Mag. and Atmosph. Elect., 33, 151-157.

Fowle, F. E., 1929: Atmospheric ozone: its relation to some solar and terrestrial phenomena. Smiths Misc. Collection, 81, no. 11.

Haurwitz, B., 1938: Atmospheric ozone as a constituent of the atmosphere. BAMS, 19, 417-424.

Inn, E. C. Y., and Y. Tanaka, 1953: Absorption coefficients of ozone in the ultraviolet and visible regions. J. Opt. Soc., 43, 870-873.

Kulkarni, R. N., P. D. Angreji, and K. R. Ramanathan, 1959: Comparison of ozone amounts measured at Delhi (28 1/2°N), Srinagar (34°N) and Tateno (35°N) in 1957-58. Papers in Meteor. and Geophys., Met. Res. Inst., X, 85-92.

Ny, T. Z., and S. P. Choong, 1932: L'absorption de la lumiére par l'ozone entre 3050 et 3400 Å (region des bandes des Huggins). Comptes Rendus, 195, 309-311.

Perl, G., and H. Dütsch, H., 1958: Die 30 jahrige Aroser Ozonmessreihe. Annalen der Schweizerischen Meteorologiskhe Zentralanstalt, No. 8.

Vigroux, E., 1953: Contribution a l'étude expèrimentale de l'absorption de l'ozone. Annales de Physique, 8, 709-762.

Wahl, E. W., 1958: Mean monthly 300 and 200 mb contours and 500, 300 and 200 mb temperatures for the Northern Hemisphere. Geophys. Res. Paper, No. 57, AFCRC-TR-58-207, AD 146861.

APPENDIX A

Preliminary Data Source - Total Ozone

Data Source Reference List

Appendix A

Preliminary Data Source - Total Ozone

(Northern Hemisphere)

Data Prior to 1 July 1957

Station	Lat.	Long.	Period	Reference
Aarhus, Denmark	5618N	1037E	Sep 51-Nov 53	18
			Mar 54-Jun 57	18
Abisko, Sweden	6820N	1847E	Jul 26, Apr-Sep 27	10
			Dec 34, Jan-Mar 35	2
Ahmedabad, India	2304N	7238E	Jan-Apr 55	13
Albuquerque, New Mexico	3503N	10637W	Jan-Jul 54	22
Aldergrove North Ireland	5439N	0613W	Jan 52-Oct 56	18
			Jan -Apr 57	18
Arosa, Switzerland	4647N	0941E	Jul 26-Jun 29	19
			Jul-Aug 30	19
			Aug 31-Sep, Nov 53	19
			Mar 54-Jun 57	19
Bismarck, North Dakota	4646N	10045W	Jan 54-Nov 56	22
Bombay, India	1855N	7254E	Oct 36-Sep 38	6
Cagliari, Sardinia	3914N	0906E	Oct 54-Nov 55	18
			Jan-Feb 56	18
			Jul 56-Jun 57	18
Camborne, England	5013N	0519W	Nov 50-May 56	18
			Oct 56-Jun 57	18
College, Alaska	6444N	14730W	Apr-Oct 52	5
			Feb-Oct 53	5
			Feb-Oct 54	5

Station	Lat.	Long.	Period	Reference
Dombas, Norway	6208N	0908E	Mar-Nov 40	16
			Feb-Nov 41	16
			Mar-Sep 42	16
			Jan-Dec 43	16
			Mar 44-Jun 46	16
Downham Market England	5236N	0023E	Nov 50-Nov 51	18
Edmonton, Canada	5334N	11331W	Aug 50-Dec 52	12
Eskdalemiur Scotland	5519N	0312W	Jun 57	18
Flagstaff, Arizona	3508N	11140W	Sep 54-Dec 56	1
Fort Worth, Texas	3250N	9703W	Jan 54-Nov 55	22
Gulmarg, India	3403N	7224E	Jun-Dec 55	13
			Apr-Sep 56	13
Helwan, Egypt	2952N	3118E	Sep 28-May 29	9
			Jul-Oct 29	9
Hemsby, England	5241N	0141E	Nov-51-Aug 52	18
			Nov 52-Sep 55	18
Kabul, Afghanistan	3432N	6910E	Jan-Dec 51	15
Kodaikanal, India	1014N	7728E	Sep 28-Aug 29	9
Lerwick, Scotland	6008N	0111W	Jul-Sep 26	7
			Mar-Oct 27	7
			May-Aug 51	18
			Mar 52-Nov 54	18
			Jan 55-Jun 57	18
Lindenberg, Germany	5212N	1408E	Jul-Oct 26	10
			Apr-Oct 27	10
Magny Les Hameaux, France	4844N	0204E	Jan 55-Jun 57	18
Marseille, France	4317N	0522E	Jan-Dec 27	3
			Jan-Dec 28	4
Messina, Sicily	3812N	1533E	Jul 54-Jun 57	18
Mount Abu, India	2436N	7243E	Jan 55-Jun 57	13

Station	Lat.	Long.	Period	Reference
New Delhi, India	2838N	7713E	Nov 45-Mar 47	14
			Jan 55-Jun 57	13
New York, N. Y.	4046N	7346W	Jan 41-Nov 42	8
			Jan-Jul 43	8
			Oct 43-Dec 44	8
Oslo, Norway	6005N	1000E	Jul 46-Apr 49	16
Oxford, England	5146N	0116W	Feb-Nov 25	7
			Feb-Oct 26	10
			Mar-Oct 27	10
			Mar -Oct 28	10
			Nov 50-Jun 57	18
Pasadena, Calif.	3409N	11810W	Sep-Dec 39	7
			Feb-Mar, May-Aug 40	7
Potsdam, Germany	5223N	1304E	Feb-Apr, Jun 42 Jan-Mar, May, Aug Sep 43	
Reykjavik, Iceland	6408N	2154W	Feb-Oct 52	18
			Feb-Oct 53	18
			Feb-Oct 54	18
			Mar-Jul 55	18
Rome, Italy	4154N	1228E	Apr 54-Jun 57	18
Santa Maria, Arores	3655N	2510W	Jun, Jul 51	18
			Jan 53-Jul 56	18
Shanghai, China	3111N	12129E	Jan-32-Dec 33	17a
			Jan 34-Dec 36	17b
			Jan -Dec 37	17c
			Feb 38-Dec 42	17c
Spitzbergen, Norway	7800N	1500E	Jul-Aug 29	7
			Nov 50-Sep 51	18
			Dec 51-Aug 53	18
			Nov 53-Oct 54	18
			Dec 54	18
			Mar-Sep 55	18
			Mar-Aug 56	18
Srinagar, India	3405N	7450E	Jan-Apr 56	13
			Nov 56-Jun 57	13

Station	Lat.	Long.	Period	Reference
Table Mountain, California	3424N	11742W	Aug 28-Aug 29	9
Tateno, Japan	3603N	14008E	Jul 55-Nov 56	20
			Feb-Jun 57	20
Tromso, Norway	6940N	1857E	Jul 35-Oct 36	21
			Jan-Dec 37	21
			Mar-Oct 38	21
			Mar 39-Dec 42	21
			Jan 43-Nov 46	16
			Jan 47-Nov 48	16
			Jan, Mar-May 49	16
			Mar 51, Dec 52	18
			Apr-Oct 53	18
			Feb-Oct 54	18
			Feb-Oct 55	18
			Feb-Jun 56	18
Uccle, Belgium	5048N	0421E	Sep 51-Aug 52	18
			Mar 54-Oct 55	18
			Apr-Jun 57	18
Uppsala, Sweden	5952N	1737E	Jul-Oct 51	18
			Mar 52-Nov 54	18
			Jan 55-Jun 57	18
Valentia, Ireland	5156N	1015W	Sep-Oct 26	10
			Mar-Oct 27	10
Washington, D.C.	3851N	7702W	Feb 48-Mar 50	11
			Jan 54-Sep 56	22

Data Source Reference List

Total Ozone

1. Adel, A. (1958): VODARO Parameters 1953-1957. Scientific Report HB 5 Contract AF 19(604)-2177 Atmospheric Research Observatory, Arizona State College, Flagstaff, Arizona.

2. Barbier, D., and Chalonge, D. (1939): Recherches sur l'ozone atmosphèrique. Journal de Physique et Radium, Ser. 7, 10, 113-123.

3. Buisson, H. (1928): Mesures de l'ozone de la haute atmosphère pendant l'année 1927. Comptes Rendus Academie des Sciences, Paris, 186 1229-1230.

4. Buisson, H. (1929): Mesures del'ozone de la haute atmosphère pendant l'annee 1928. Comptes Rendus Academie des Sciences, Paris, 188, 647-648.

5. Cain, J.C and Cain, A. B. (1955): Atmospheric ozone at College, Alaska. University Geophysical Institute, Contract AF 19(604)-127. Final Report March 1955.

6. Chiplonkar, M.W.(1939): Measurement of atmospheric ozone at Bombay. Proceedings Indian Academy of Science, 10, 105-120.

7. Craig, R.A. (1950): The observation and photochemistry of atmospheric ozone and their meteorological significance. Meteorological Monographs American Meteorological Society, v. 1, no. 2.

8. Culnan, R.N. (1945): Ozone measurements at New York University and their relation to certain meteorological conditions. Department of Meteorology, College of Engineering, New York University, New York. (Unpublished.)

9. Dobson, G.M.B. (1930): Observation of the amount of ozone in the earth's atmosphere and its relation to other geophysical conditions, part IV. Proceedings Royal Society, London, A 129, 411-433.

10. Dobson, G.M.B., Harrison, D.C., and Lawrence, J.(1928): Measurement of the amount of ozone in the earth's atmosphere and its relation to other geophysical conditions, Part III. Proceedings Royal Society, London, A 122, 456-486.

11. Fritz, S., and Stevens, G.C.(1950): Atmospheric ozone at Washington, D. C. Monthly Weather Review, 78(8), 135-147.

12. Gowan, E.H., and Leppard, R.D. (1953): Meteorological variations in the quantity of atmospheric ozone over Edmonton, Canadian Journal of Physics, 31, 702-713.

13. Indian Journal of Meteorology and Geophysics (Quarterly) 6, no. 3, through 11, no. 2.

14. Karandikar, R.V. (1948): Studies in atmospheric ozone Proceedings Indian Academy of Science 28A, 63.

15. Khalek, A. (1954): Variation Diurne et Annuelle de L'Eppaisseur Réduite et de la température Moyenne de L'ozone atmospherique a kaboul. Journal Scientifique de la Meteorologie 6 85-118.

16. Langlo, K. (1952): On the amount of atmospheric ozone and its relation to meteorological conditions. Geofysiske Publikasjoner, 18, No. 6.

17. Lejay, P. (1934): Measures de la quantité d'ozone contenue dans l'atmosphère a l'observatoire de Zo-se. Notes de Météorologie Physique. Observatoire de Zi-Ka-We, Shanghai

(a) Fascicule III, 1934
(b) Fascicule VII, 1937
(c) Fascicule X, 1948.

18. Norman, C.W.B.: Total ozone values for selected European stations. International Ozone Commission. (Unpublished).

19. Perl, G. and Dütsch, H. (1959): Die 30 jahrige Aroser Ozonmessreihe. Annalen der Schweizerischen Meteorologische Zentralanstalt No. 8.

20. Tateno, Japan. Aerological Observatory (1957): Observations of the total amounts of ozone over Tateno. Journal of Aerology Observatory 6(1). 17-35 and 6 no. 2.

21. Tonsberg, E. and Olsen, K.L. (1944): Investigation on atmospheric ozone at Nordlysobservatoriet, Tromso, Geofysiske Publikasjoner 13, no. 12.

22. United States Weather Bureau. Climatological Data - National Summary, 5, 6, 7.

APPENDIX B

Monthly means of observed total ozone (Dobson units - 10^{-3} cm NTP). All values have been converted to be consistent with Vigroux absorption coefficients. Number of days of observations for each month is indicated when available.

Aarhus, Denmark, 56°18'N, 10°37'E

Year	Jan	Feb	Mar	Apr	May	Jun	Jul	Aug	Sep	Oct	Nov	Dec
									21	30	24	31
1951									287	264	269	314
	28	27	23	29	28	28	27	26	26	20	29	27
1952	369	388	443	424	416	407	352	318	321	332	309	362
	28	21	31	24	25	26	20	27	18	27	21	
1953	344	386	382	390	405	389	378	339	292	296	283	
			17	28	30	27	28	28	26	23	22	26
1954			416	454	419	393	392	366	340	303	298	306
	29	27	29	28	28	27	30	31	23	25	22	24
1955	352	446	431	411	420	397	356	359	313	306	279	321
	26	27	27	24	19	28	30	25	28	25	25	28
1956	350	426	397	393	420	392	360	374	313	305	303	290
	24	22	27	29	28	20						
1957	326	445	397	408	426	378						

Abisko, Sweden, 68°20'N, 18°47'E

							8					
1926							301					
				2	14	7	9	5	7			
1927				449	424	347	321	313	286			
1928												
1929												
1930												
1931												
1932												
1933												
											3	
1934											237	
	11	12	6									
1935	296	363	356									

Ahmedabad, India, 23°04'N,72°38'E

	28	26	30	29
1955	222	227	235	242

Albuquerque, New Mexico, 35°03'N, 106°37'W

Year	Jan	Feb	Mar	Apr	May	Jun	Jul	Aug	Sep	Oct	Nov	Dec
	17	22	14	4	16	17	3					
1954	307	328	352	354	362	332	326					

Aldergrove, N. Ireland, 54°39'N, 06°13'W

	4	26	29	30	18	21	31	31	29	26	28	27
1952	400	339	416	397	385	355	335	326	303	296	267	298
	28	26	31	30	31	29	29	13	26	31	29	25
1953	286	324	343	375	364	362	359	343	288	282	260	295
	27	21	31	30	30	30	30	30	30	29	27	22
1954	330	375	367	407	407	390	370	345	313	287	280	276
	23	23	30	28	31	29	31	30	30	31	28	19
1955	325	416	377	358	397	381	351	328	291	287	261	305
	18	25	21	26	28	24	24	23	17	7		
1956	335	348	384	394	396	377	369	374	314	290		
	12	14	19	9								
1957	314	409	397	381								

Arosa, Switzerland, 46°47'N, 09°41'E

Year	Jan	Feb	Mar	Apr	May	Jun	Jul	Aug	Sep	Oct	Nov	Dec
							5	28	27	25	20	13
1926							303	292	275	268	286	313
	19	24	24	18	31	27	30	29	26	29	22	23
1927	351	351	362	360	367	337	326	298	294	273	275	305
	19	21	17	21	19	28	29	26	19	21	17	22
1928	313	313	335	347	360	318	296	286	277	258	271	302
	20	25	22	25	18	6	---- no observations -------					
1929	336	386	343	401	354	333						
							1	11				
1930	---no observations ----------						(279)	286	--- no obs. -------			
								7	20	19	14	21
1931	---no observations ----------							301	324	273	277	291
	22	25	19	11	19	22	16	24	15	16	16	12
1932	307	335	356	378	347	335	322	290	283	286	283	272
	14	15	24	13	16	21	27	24	21	7	11	21
1933	344	350	384	366	374	359	322	307	298	302	301	325
	12	20	19	23	21	17	24	19	21	17	19	12
1934	322	310	377	345	350	343	317	310	272	277	282	287
	10	12	21	18	23	20	17	8	14	11	12	14
1935	320	374	354	369	360	309	320	301	279	267	290	302
	12	18	19	14	15	18	19	24	20	21	16	23
1936	317	371	382	369	359	339	317	305	292	299	287	296
	14	10	21	15	22	19	16	15	16	8	18	15
1937	333	339	379	367	352	337	313	311	291	273	271	343
	13	21	23	21	14	15	19	8	20	20	25	17
1938	325	355	314	377	370	324	314	314	286	270	276	288
	14	19	12	11	6	16	22	12	14	17	20	17
1939	309	329	370	335	367	326	320	302	277	294	275	299
	20	13	26	24	23	21	19	21	19	10	17	21
1940	373	385	401	412	388	373	333	311	299	282	291	325
	19	21	22	21	22	26	23	27	25	21	21	20
1941	348	379	400	393	401	347	336	324	295	290	298	298
	19	20	20	18	24	21	24	24	27	19	19	25
1942	385	405	359	392	362	335	314	298	275	264	288	302
	15	15	29	26	22	22	21	22	24	27	13	18
1943	325	329	370	350	336	339	324	292	271	283	292	309
	20	16	13	21	24	25	24	26	24	24	15	25
1944	290	351	370	347	336	337	309	295	282	284	288	309
	23	20	23	26	28	29	29	28	22	27	23	9
1945	363	347	347	359	362	339	317	316	287	279	286	302

(Cont.)

Arosa, Switzerland (Continued)

Year	Jan	Feb	Mar	Apr	May	Jun	Jul	Aug	Sep	Oct	Nov	Dec
	24	18	26	25	25	22	24	16	22	28	24	16
1946	324	339	366	348	341	330	306	296	268	282	287	306
	25	19	21	25	27	24	25	30	28	28	19	14
1947	369	382	378	355	348	329	322	313	296	287	269	301
	20	20	27	26	28	23	21	27	16	24	22	25
1948	329	356	335	350	340	333	332	301	288	272	276	310
	14	26	26	27	23	29	28	23	26	27	17	20
1949	321	351	363	344	356	341	324	310	275	264	286	283
	22	20	27	23	28	27	31	24	25	25	19	17
1950	340	351	352	367	360	341	311	305	283	279	277	328
	20	20	24	29	26	26	26	26	26	30	18	24
1951	326	386	400	382	369	351	320	310	287	288	269	301
	21	22	21	23	25	27	30	27	25	19	18	17
1952	363	369	394	371	370	345	329	309	306	287	292	321
	25	25	30	26	24	22	26	22	25	3	25	no
1953	324	362	359	367	367	345	316	306	283	(269)	258	obs
			23	16	24	12	25	22	12	25	24	13
1954	-no obs-		-360	400	374	348	335	317	295	276	282	275
	21	11	27	24	23	26	18	28	23	24	24	11
1955	305	360	384	359	348	339	328	321	290	283	269	299
	17	22	21	17	21	11	23	12	23	23	21	20
1956	325	381	363	374	348	343	315	296	277	274	275	294
	21	23	29	24	19	26						
1957	325	328	338	354	367	335						

Bismarck, N. Dak., 46°46'N,100°45'W

	22	22	21	19	25	21	29	30	24	26	25	25
1954	360	363	408	416	405	363	359	359	326	307	280	321
	23	18	26	18	23	25	26	28	25	29	21	23
1955	347	373	422	358	324	370	341	316	299	272	284	288
	21	19	25	25	24	26	28	28	24	30	21	
1956	295	362	375	394	359	345	345	329	306	282	287	

Bombay, India, 18°55'N, 72°54'E

Year	Jan	Feb	Mar	Apr	May	Jun	Jul	Aug	Sep	Oct	Nov	Dec
										10	2	9
1936										260	235	256
	26	17	29	28	3	2	4	14	15	28	22	31
1937	257	280	252	262	228	226	215	233	256	262	246	248
	30	28	31	27	28	9	11	10	16			
1938	246	256	257	275	268	264	267	248	256			

Cagliari, Sardinia, 39°14'N, 09°06'E

										31	30	31
1954										295	299	292
	30	27	28	28	31	30	31	30	30	31	27	
1955	302	321	356	370	321	324	316	314	303	292	313	
	9	17					31	30	30	27	27	31
1956	313	385					314	301	299	294	301	302
	29	28	31	27	30	28						
1957	310	301	321	318	366	337						

Camborne, England, 50°13'N, 05°19'W

											16	25
1950											292	318
	29	27	26	28	31	26	28	30	28	2	5	24
1951	329	382	385	366	409	360	320	326	282	275	271	307
	21	24	26	27	28	28	30	29	28	26	23	23
1952	354	340	397	394	423	392	360	347	335	305	286	302
	20	25	30	26	26	17	27	27	25	29	27	30
1953	301	333	366	396	384	371	355	324	283	284	264	280
	27	27	28	29	29	26	29	29	27	27	24	27
1954	320	362	366	405	394	381	355	339	301	282	277	276
	28	23	29	26	24	27	29	28	26	26	29	28
1955	317	377	378	352	379	362	344	324	282	271	257	295
	25	29	29	19	8					26	25	27
1956	326	350	350	378	348					264	262	275
	27	25	28	30	30	30						
1957	301	359	325	333	350	333						

College, Alaska , 64°44'N, 147°30'W

Year	Jan	Feb	Mar	Apr	May	Jun	Jul	Aug	Sep	Oct	Nov	Dec
				9	17	19	13	16	3	6		
1952				446	411	356	326	301	299	299		
		5	25	27	22	18	20	6	13	11		
1953		396	438	416	394	351	287	282	282	326		
		10	18	15	18	25	19	22	13	8		
1954		427	437	449	411	394	370	330	296	295		

Dombas, Norway, 62°08'N, 09°08'E

			9	19	22	12	10	20	24	24	6	
1940			390	392	384	322	311	305	295	264	290	
		6	23	28	25	23	18	25	27	22	3	
1941		416	422	422	393	324	306	318	264	287	275	
			15	24	23	24	30	28	10			
1942			400	364	362	347	332	301	275			
	13	9	19	26	30	19	27	25	26	30	26	22
1943	290	307	373	379	369	322	314	302	273	250	269	305
			4	23	27	27	22	20	30	27	23	17
1944			363	356	358	329	302	269	283	258	269	292
	7	4	24	29	22	26	29	30	29	28	24	22
1945	311	367	367	398	386	340	305	291	277	248	253	313
	29	17	27	29	31	17						
1946	318	333	386	374	254	336						

Downham Market, England, 52°36'N, 00°23'E

											26	31
1950											302	326
	28	25	31	29	31	29	31	31	29	30	17	
1951	352	420	419	420	423	394	363	350	295	291	280	

Edmonton, Alberta, Can., 53°34'N, 113°31'W

								15	16	5	9	10
1950								310	264	283	307	295
	14	16	21	18	20	18	26	23	24	23	21	12
1951	333	343	405	359	389	401	354	330	292	290	294	322
	20	25	23	21	22	18	21	20	25	29	23	21
1952	371	398	419	398	384	350	336	321	286	268	307	299

Flagstaff, Arizona, 35°08'N, 111°40'W

Year	Jan	Feb	Mar	Apr	May	Jun	Jul	Aug	Sep	Oct	Nov	Dec
									22	24	17	14
1954									268	252	257	279
	11	14	19	17	16	22	23	15	24	22	13	7
1955	275	287	290	309	306	292	279	283	267	254	252	250
	7	10	19	7	20	17	10	19	16	13	6	10
1956	282	311	306	321	306	288	279	277	267	261	245	275

Fort Worth, Texas, 32°50'N, 97°03'W

	16	26	22	19	19	27	26	27	28	17	24	21
1954	273	294	294	303	328	316	299	283	269	253	254	265
	12	18	19	20	24	26	26	25	28	27	7	
1955	276	265	269	283	298	298	292	284	269	253	267	

Gulmarg, India, 34°03'N, 72°24'E

						18	21	25	28	26	28	24
1955						258	243	230	233	235	235	249
				2	30	24	25	22	25			
1956				280	257	256	250	224	222			

Helwan, Egypt, 29°52'N, 31°18'E

									3	9	16	22
1928									256	256	248	253
	23	18	15	17	2		8	20	23	6		
1929	279	283	299	294	284		275	276	277	257		

Hemsby, England, 52°41'N, 01°41'E

											7	23
1951											269	314
	26	27	28	29	31	30	31	12			16	30
1952	375	360	423	415	415	418	369	354			302	314
	31	27	31	30	29	30	31	30	29	24	19	27
1953	298	348	358	382	362	375	354	316	288	280	261	296
	22	20	27	30	28	30	30	27	27	22	23	8
1954	325	397	378	412	400	373	360	339	310	280	273	299
	26	20	25	25	18	24	30	30	17			
1955	321	401	374	348	384	367	344	317	284			

Kabul, Afghanistan, 34°32'N, 69°10'E

Year	Jan	Feb	Mar	Apr	May	Jun	Jul	Aug	Sep	Oct	Nov	Dec
	6	10	8	10	4	5	10	18	20	13	10	11
1951	(273)	268	(314)	321	(308)	(236)	249	282	260	291	271	347

Kodaikanal, India, 10°14'N, 77°28'E

									17	12	7	12
1928									246	242	231	226
	24	24	23	15	18	7	14	19				
1929	230	233	238	245	253	250	253	245				

Lerwick, Scotland, 60°08'N, 01°11'W

							21	17	15			
1926							328	321	301			
			12	13	17	14	22	20	19	5		
1927			416	416	397	341	333	335	305	307		
					5	26	30	18				
1951					359	362	355	336				
			16	30	31	30	31	31	30	31	22	3
1952			420	404	389	398	352	337	310	302	256	250
	6	27	31	30	31	30	30	31	30	30	16	4
1953	292	337	355	393	382	366	354	326	287	273	280	246
	4	27	31	29	31	30	31	29	29	30	14	
1954	318	370	385	411	385	364	352	329	310	288	284	
	1	27	25	30	7	2	27	31	25	30	17	2
1955	291	404	378	355	385	371	325	306	291	273	248	260
	3	28	30	30	31	30	31	31	30	31	17	1
1956	290	313	384	409	381	378	344	348	302	277	260	248
	5	23	31	30	31	30						
1957	313	438	401	381	407	369						

Lindenberg, Germany, 52°12'N, 14°08'E

							23	22	19	10
1926							320	320	294	295
				7	26	22	20	19	13	7
1927				381	403	367	335	313	316	301

Magny Les Hameaux, France, 48°44'N, 02°04'E

Year	Jan	Feb	Mar	Apr	May	Jun	Jul	Aug	Sep	Oct	Nov	Dec
	7	15	15	20	20	19	14	7	17	17	17	11
1955	298	354	340	335	347	336	343	297	273	271	253	273
	19	18	21	12	11	19	17	12	15	17	17	11
1956	339	369	356	381	328	337	317	340	284	288	284	295
	17	14	15	16	14	5						
1957	326	351	326	350	369	366						

Marseille, France, 43°17'N, 05°22'E

	3	17	14	29	19	24	29	27	22	24	11	7
1927	370	389	422	432	424	378	354	330	330	321	273	316
	20	22	13	17	26	24	30	14	22	21	23	19
1928	343	378	412	405	394	351	336	313	316	313	326	354

Messina, Italy, 38°12'N, 15°33'E

							31	31	30	31	30	31
1954							287	284	279	271	272	275
	31	28	31	30	31	30	31	31	29	30	30	31
1955	282	280	317	335	305	298	294	284	276	267	265	276
	31	27	30	28	30	25	30	31	28	29	28	30
1956	301	354	330	341	326	340	311	292	275	265	261	303
	31	28	30	30	31	30						
1957	344	332	378	397	407	351						

Mount Abu, India, 24°36'N, 72°43'E

	31	27	31	30	29	27	27	11	12	29	25	30
1955	222	227	233	241	252	246	243	243	246	242	238	231
	31	29	31	27	31	24	1	9		24	11	31
1956	237	254	254	258	256	248	246	230		230	231	224
	30	27	30		6	23						
1957	219	219	242		268	248						

New Delhi, India, 28°38'N, 77°13'E

Year	Jan	Feb	Mar	Apr	May	Jun	Jul	Aug	Sep	Oct	Nov	Dec
											19	27
1945											230	231
	28	22	28	30	29	28	21	21	28	21	29	28
1946	231	235	249	256	254	257	243	235	239	243	238	248
	18	26	24									
1947	261	268	269									
1948												
1949												
1950												
1951												
1952												
1953												
1954												
	28	27	31	30	30	22	25	25	28	26	30	31
1955	264	257	248	257	[illegible]2	253	256	250	249	257	246	256
	28	29	31	30	29	26	21	25	28	27	29	31
1956	275	283	277	262	264	260	269	279	265	237	234	241
	25	28	30	29	31	28						
1957	250	235	242	233	243	256						

New York, N. Y., 40°46'N, 73°46'W

	24	27	26	28	31	26	28	31	30	30	25	30
1941	366	417	431	388	411	390	374	358	324	308	311	325
	25	22	10	17	13	4	14	24	21	5	3	
1942	384	405	420	418	388	373	354	340	307	335	325	
	19	8	10	16	19	21	11	357	343	11	13	13
1943	363	386	389	400	385	333	371	msg	msg	330	315	339
	20	23	23	17	19	26	31	24	24	26	22	23
1944	356	384	358	408	371	362	364	348	317	311	325	324

Oslo, Norway, 60°05'N, 10°00'E

							5	3	22	26	21	23
1946							333	295	276	241	261	290
	26	24	26	27	27	25	27	26	29	26	25	26
1947	284	431	430	388	350	343	326	282	282	272	276	337
	27	25	27	30	30	28	27	23	25	18	10	4
1948	420	262	351	378	360	340	322	316	277	268	260	351
	15	20	26	23								
1949	326	355	355	377								

Oxford, England, 51°46'N, 01°16'W

Year	Jan	Feb	Mar	Apr	May	Jun	Jul	Aug	Sep	Oct	Nov	Dec
		8	16	24	30	29	14	20	23	18	21	
1925		424	382	424	403	373	364	356	336	305	295	
		10	25	21	27	28	25	27	25	22		
1926		333	347	358	375	367	318	309	273	277		
			25	29	30	24	24	25	10	17		
1927			408	384	382	373	345	329	305	283		
			11	20	19	19	24		24	12		
1928			354	386	379	352	310		291	286		
											16	31
1950											303	320
	31	28	31	30	31	30	31	31	29	31	30	31
1951	336	403	393	390	397	359	321	324	276	269	268	301
	31	29	31	30	31	30	31	31	30	31	30	31
1952	355	333	393	385	378	367	336	322	311	296	282	303
	31	28	31	30	31	30	31	31	30	31	30	30
1953	303	345	355	379	355	364	340	307	283	279	268	313
	30	28	31	30	31	30	31	31	30	31	30	26
1954	344	392	367	398	385	347	337	318	294	273	275	280
	30	28	31	27	31	30	31	31	30	31	30	29
1955	320	392	370	326	358	344	339	313	283	284	272	310
	30	29	31	30	31	30	31	31	30	31	30	30
1956	350	369	373	389	362	358	341	340	294	286	280	286
	29	25	31	30	31	30						
1957	313	385	350	363	379	356						

Pasadena, Calif., 34°09'N, 118°10'W

1939									306	306	286	286
1940		347	354		354	347	326	279				

Potsdam, Germany

1942		398	373	400		339						
1943	377		345		379			279	256			

Reykjavik, Iceland, 64°08'N, 21°54'W

Year	Jan	Feb	Mar	Apr	May	Jun	Jul	Aug	Sep	Oct	Nov	Dec
		3	9	13	20	16	24	21	8	1		
1952		341	423	409	398	370	345	330	325	288		
		3	16	13	30	23	28	21	21	10		
1953		351	394	400	398	379	359	336	303	307		
		3	28	28	30	30	28	31	29	21		
1954		400	418	443	415	384	367	345	314	299		
			13	28	30	29	31					
1955			398	392	394	377	354					

Rome, Italy, 41°54'N, 12°28'E

				30	31	30	31	31	30	31	29	31
1954				389	378	321	303	294	275	273	277	276
	31	27	29	30	31	30	31	31	30	31	30	31
1955	295	332	340	358	324	321	320	303	291	292	271	290
	31	27	29	28	28	29	31	31	29	29	27	31
1956	326	382	348	360	348	366	325	311	292	295	305	316
	30	28	31	26	31	30						
1957	333	322	350	362	366	332						

Santa Maria, Azores, 36°55'N, 25°10'W

						27	3					
1951						318	330					
1952												
	8	28	31	24	30	30	31	31	30	31	30	31
1953	294	311	345	356	343	341	306	299	279	271	275	283
	29	28	31	30	30	30	29	26	30	22	30	30
1954	295	321	336	356	364	329	320	298	290	279	280	287
	29	28	27	30	31	30	31	31	27	31	29	31
1955	271	292	330	344	329	321	321	305	292	275	287	279
	28	29	31	30	31	30	29					
1956	313	322	328	351	360	332	317					

Shanghai, China, 31°11'N, 121°29'E

Year	Jan	Feb	Mar	Apr	May	Jun	Jul	Aug	Sep	Oct	Nov	Dec
	15	15	10	14	12	9	23	14	14	14	13	15
1932	288	330	356	339	328	326	307	311	317	307	301	298
	6	4	8	9	13	5	16	16	16	5	8	11
1933	345	358	356	345	347	352	316	325	314	288	280	314
	12	12	12	7	10	9	18	10	8	16	7	9
1934	341	337	364	339	337	326	317	306	301	294	268	296
	12	6	12	4	12	5	9	3	10	12	9	10
1935	344	374	356	356	356	332	305	305	310	298	283	305
	6	7	8	7	6	3	10	12	20	21	13	5
1936	360	366	374	366	363	284	310	316	313	303	291	301
	10	9	9	13	18	15	23	22	12	19	9	14
1937	318	343	351	362	360	335	318	302	302	296	302	322
		11	10	15	11	6	16	22	15	16	24	15
1938		363	362	381	355	333	317	307	292	292	299	320
	17	10	12	13	16	13	13	17	20	12	14	24
1939	321	325	348	363	352	336	320	299	310	305	303	320
	14	12	11	13	12	12	21	18	15	16	17	17
1940	348	364	384	385	360	363	320	324	310	303	302	318
	21	13	17	18	15	17	16	16	10	20	16	15
1941	335	340	351	364	363	354	324	314	314	317	313	316
	22	7	16	17	15	8	21	7	11	15	18	4
1942	321	360	352	379	377	343	326	302	303	307	309	313

Srinagar, India, 34°05'N, 74°50'E

	16	27	24	24							6	25
1956	283	280	272	267							243	254
	16	22	22	21	21	29						
1957	275	264	268	275	282	273						

Spitzbergen, Norway, 78°N 15°E

Year	Jan	Feb	Mar	Apr	May	Jun	Jul	Aug	Sep	Oct	Nov	Dec
							22	21				
1929							347	317				
											5	7
1950											310	306
	5	2	6	13	8	8	12	8	1			4
1951	377	458	481	442	400	367	317	290	292			330
	4	3	5	18	14	12	31	26	17	5	1	3
1952	329	398	513	434	404	351	329	303	291	287	231	375
	7	7	25	21	26	29	25	23			4	1
1953	404	396	407	428	388	328	302	277			231	400
	4	11	31	25	30	25	25	31	27	26		3
1954	378	409	450	442	381	363	328	287	256	273		286
			6	29	28	30	30	31	30			
1955			396	396	392	356	318	296	276			
			4	27	30	29	31	26				
1956			408	434	386	347	301	284				

Table Mountain, Calif., 34°24'N, 117°42'W

								31	30	30	29	29
1928								264	252	257	252	277
	21	22	26	29	29	27	30	22				
1929	294	317	326	335	313	287	277	275				

Tateno, Japan, 36°03'N, 140°08'E

							23	10	15	16	23	25
1955							280	273	268	246	268	287
	22	21	17	20	13	13	2	16	18	15	19	
1956	322	348	337	348	320	311	314	287	273	261	258	
		6	29	30	30	29						
1957		355	375	356	351	343						

Tromso, Norway, 69°40'N, 18°57'E

Year	Jan	Feb	Mar	Apr	May	Jun	Jul	Aug	Sep	Oct	Nov	Dec
							8	17	25	17	5	2
1935							317	271	267	227	257	258
	9	7	17	25	28	24	25	27	18	16		
1936	233	269	404	419	374	343	322	294	279	265		
	6	2	18	23	16	19	28	22	22	2	4	4
1937	339	447	430	358	339	322	294	279	276	279	230	273
			17	17	19	19	18	24	5	4		
1938			394	426	382	343	294	295	287	268		
			21	24	21	24	31	26	29	30	30	18
1939			367	374	371	344	303	273	276	288	295	201
	17	18	25	24	27	23	31	31	30	31	28	19
1940	384	435	441	445	392	369	344	326	299	282	242	227
	22	28	31	30	31	30	31	31	30	30	30	15
1941	352	443	469	443	412	374	317	306	287	292	271	296
	18	28	31	30	31	30	31	31	30	31	30	31
1942	335	461	492	431	412	354	325	310	299	288	239	211
	31	28	31	30	31	30	31	31	30	29	23	16
1943	280	397	413	412	401	344	454	307	283	264	241	169
	19	28	30	30	31	30	31	28	30	31	27	30
1944	180	379	403	400	382	336	299	292	294	284	250	181
	31	28	31	30	31	30	30	31	30	31	30	26
1945	226	373	398	432	397	358	302	301	295	287	224	177
	25	27	31	30	31	30	29	31	29	27	18	
1946	197	366	420	426	385	333	299	287	273	248	205	
	15	23	31	30	31	30	31	30	30	30	27	5
1947	167	384	409	404	389	344	317	299	292	288	208	147
	10	26	31	30	31	30	31	31	30	29	9	
1948	253	348	378	405	390	350	311	309	286	272	246	
	28		29	29	20							
1949	333		369	420	409							
1950												
			13	14	10	9	4	6	5	2	5	2
1951			487	428	409	360	325	288	275	242	280	393
	3	3	12	13	14	21	18	11	9	19	3	2
1952	351	413	460	431	404	359	317	313	307	298	318	379

(Cont.)

Tromso, Norway (Cont.)

Year	Jan	Feb	Mar	Apr	May	Jun	Jul	Aug	Sep	Oct	Nov	Dec
				28	31	30	29	30	29	30		
1953				415	385	322	311	290	261	252		
		26	31	28	28	29	30	31	29	30		
1954		398	427	430	382	358	309	292	290	272		
		24	29	28	31	30	31	31	30	29		
1955		456	437	416	393	364	313	294	268	250		
		26	27	29	29	25						
1956		333	377	431	364	337						

Uccle, Belgium, 50°48'N, 04°21'E

									7	25	13	21
1951									258	257	262	302
	18	20	26	26	23	19	11	11				
1952	388	358	393	389	390	356	348	305				
1953												
			14	17	19	19	18	18	14	9	16	6
1954			360	396	374	347	335	301	283	253	252	277
	4	4	9	16	14	9	7	4	5	7		
1955	326	362	359	329	350	337	321	310	250	267		
1956												
				7	1	3						
1957				356	360	302						

Uppsala, Sweden, 59°52'N, 17°37'E

Year	Jan	Feb	Mar	Apr	May	Jun	Jul	Aug	Sep	Oct	Nov	Dec
							23	16	10	6		
1951							350	307	287	250		
			18	20	27	20	21	22	22	28	21	16
1952			449	383	403	393	340	335	314	324	276	335
	13	24	31	30	31	30	31	31	29	30	30	8
1953	309	373	364	385	398	358	359	330	287	279	269	282
	24	28	30	30	30	29	26	21	26	30	23	
1954	360	394	401	426	390	367	359	322	317	295	282	
	20	20	28	28	29	26	30	28	27	25	24	17
1955	325	421	416	401	394	359	329	306	296	286	287	314
	17	17	27	26	31	28	28	24	17	26	19	15
1956	360	351	379	415	384	358	339	341	279	288	290	292
	19	21	27	24	25	17						
1957	321	475	400	389	385	374						

Valentia, Ireland, 51°56'N, 10°15'W

									7	6		
1926									273	303		
			19	16	20	12	14	13	8	9		
1927			408	394	371	384	352	350	310	296		

Washington, D. C., 38°51'N, 77°02'W

		4	6	no	12	17	2	1	18	15	12	17
1948		288	292	obs	321	310	277	302	286	262	227	267
	8	6	12	11	15	1	17	16	14	12	12	15
1949	276	284	318	330	325	374	295	290	276	249	271	305
	9	7	5									
1950	279	333	341									
1951												
1952												
1953												
	9	17	17	19	16	15	21	21	15	17	12	16
1954	345	374	412	384	386	344	347	326	311	301	306	317
	17	16	20	12	20	20	19	18	15	16	17	4
1955	305	321	356	362	356	363	343	314	317	299	295	299
	12	14	1	24	15	3	7	10	3			
1956	337	277	281	371	329	322	326	320	268			